Atomic-Scale Design of Iron Fischer-Tropsch Catalysts:
A Combined Computational Chemistry, Experimental, and
Microkinetic Modeling Approach

1st Annual Report

Professor Manos Mavrikakis,

Professor James A. Dumesic,

Amit A. Gokhale

Rahul P. Nabar

Department of Chemical and Biological Engineering

University of Wisconsin - Madison

Madison, WI 53706

Professor Calvin H. Bartholomew,

Dr. Hu Zou,

Brian Critchfield

Department of Chemical Engineering

Brigham Young University

Provo, UT 84602

March 22, 2005

Disclaimer

Abstract

Efforts during this first year focused on four areas: (1) searching/summarizing published FTS mechanistic and kinetic studies of FTS reactions on iron catalysts; (2) construction of mass spectrometer-TPD and Berty CSTR reactor systems; (3) preparation and characterization of unsupported iron and alumina-supported iron catalysts at various iron loadings (4) Determination of thermochemical parameters such as binding energies of reactive intermediates, heat of FTS elementary reaction steps, and kinetic parameters such as activation energies, and frequency factors of FTS elementary reaction steps on a number of model surfaces. Literature describing mechanistic and kinetic studies of Fischer-Tropsch synthesis on iron catalysts was compiled in a draft review. Construction of the mass spectrometer-TPD system is 90% complete and of a Berty CSTR reactor system 98% complete. Three unsupported iron catalysts and three alumina-supported iron catalysts were prepared by nonaqueous-evaporative deposition (NED) or aqueous impregnation (AI) and characterized by chemisorption, BET, extent-of-reduction, XRD, and TEM methods. These catalysts, covering a wide range of dispersions and metal loadings, are well-reduced and relatively thermally stable up to 500-600°C in H_2, thus ideal for kinetic and mechanistic studies. The alumina-supported iron catalysts will be used for kinetic and mechanistic studies. In the coming year, adsorption/desorption properties, rates of elementary steps, and global reaction rates will be measured for these catalysts, with and without promoters, providing a database for understanding effects of dispersion, metal loading, and support on elementary kinetic parameters and for validation of computational models that incorporate effects of surface structure and promoters. Furthermore, using state-of-the-art self-consistent Density Functional Theory (DFT) methods, we have extensively studied the thermochemistry and kinetics of various elementary steps on three different model surfaces: (i) Fe(110) (ii) Fe(110) modified by subsurface C, and (iii) Fe surface modified with Pt adatoms. These studies have yielded valuable insights into the reactivity of Fe surfaces for FTS, and provided accurate estimates for the effect of Fe modifiers such as subsurface C and surface Pt.

Table of Contents

Introduction

A. Background

Fischer-Tropsch Synthesis (FTS) has been used commercially for more than 70 years in the conversion of syngas (H_2/CO), derived from primarily coal but more recently from natural gas, into liquid hydrocarbons [1,2]. Its application to production of liquid fuels from natural gas (GTL) is expanding into a large world-wide industry, while its application to conversion of syngas from renewable biomass is being researched. Gasoline and diesel fuels produced from FT synthesis are premium products of low aromaticity and zero sulfur content. Although FTS is in some respects a "mature technology", substantial improvements have been realized during the past three decades in catalyst, reactor, and process technologies as a result of intensive research. Moreover, improvements could yet be realized in catalyst and reactor design through a deeper fundamental understanding of the reaction mechanism and catalyst activity-structure relationships. Combined application of modern surface science and computational chemistry tools is a powerful methodology for realizing deeper understanding required for improving catalyst design.

Almost 80 years ago, Fischer and Tropsch postulated that CO hydrogenation takes place on bulk carbides of Co and Fe. Over the decades a consensus has emerged that FTS is a polymerization process involving addition of a CH_x (x = 0-2) monomer to a growing hydrocarbon chain. The formation of the surface CH_x is proposed to occur via adsorption of CO on a metal site and dissociation of CO to a surface carbon atom, i.e. a surface carbide ($C_{(ad)}$), followed by stepwise addition of H atoms to produce methylidyne ($CH_{(ad)}$), methylene ($CH_{2(ad)}$) methyl ($CH_{3(ad)}$) species. However, there is little quantitative information regarding the potential energies of these intermediates or the kinetic parameters for these and the subsequent elementary steps producing hydrocarbons. Moreover, there is little consensus regarding the mechanisms of C-C coupling, i.e. which of the CH_x species are involved in this important step for either Co or Fe catalysts.

Both Co and Fe catalysts have been used commercially for FTS. Fe catalysts were used for 55 years at Sasol for conversion of coal to fuels and chemicals because of their low cost and ability to process coal syngas having low H_2/CO ratios as a result of their high activities for the water gas shift reaction. For the same reason Fe catalysts are favored for production of fuels from biomass. Since Co catalysts are more productive and stable than Fe catalysts, they are presently favored in GTL processes; nevertheless, the low cost and low methane selectivity of Fe catalysts make them an attractive option, especially if more productive, stable, supported Fe catalysts can be developed. A microkineticmodel for Fe FTS could enable the needed improvements in design. There are no previously reported microkinetic studies of FTS on Fe.

This report describes progress made during the first year of a three-year DOE-sponsored project for advanced design of supported iron Fischer-Tropsch catalysts through development of a microkineticmodel for FTS based on theoretical computations and mechanistic experiments. The BYU team is assisting the computations team at U. Wisconsin through study and search of literature addressing FTS kinetics and mechanisms, experimental mechanistic studies of elementary reactions, and the development of rate data for alumina supported iron FTS catalysts.

B. Work Statement

   I. OBJECTIVES

   The principal objective of this work is to use state-of-the-art computational chemistry methods and experiments for developing and validating a detailed microkinetic model describing the rates of the important elementary steps that occur during FTS on the surface of an iron catalyst. Special emphasis is placed on the effects of potassium oxide and Cu promoters (alternatively Pt) and of surface/subsurface carbon species on these important elementary steps.

   II. SCOPE

This microkinetic model will enable prediction of catalyst activity and hydrocarbon selectivities over a range of temperatures, pressures, H_2/CO ratio, and as a function of promoter type and concentration, and of surface/subsurface carbon coverage. It will address the molecular principles governing the relative rates of chain growth versus termination on iron FT catalysts, thereby providing a basis for maximizing desirable products (e.g. diesel liquids and waxes) while minimizing formation of undesirable products such as methane, LPG, and alcohols.

   III. TASKS

   To accomplish the above objectives, the proposed research has been divided into the following specific tasks to be accomplished over a period of 36 months:

1. Task 1: Search the literature for and incorporate available kinetic parameters into a microkinetic model for FTS surface reactions on iron; determine consistency of available data and needs for obtaining additional parameters—this will be an ongoing task. **(BYU and UW)**

2. Task 2: Measure kinetic parameters for key elementary steps including CO adsorption/dissociation, H_2 dissociation, C hydrogenation, olefin adsorption on unpromoted and promoted Fe catalysts [promoted with K_2O and/or Cu (alternatively Pt)] under high pressure conditions using TPD and temperature-programmed reaction spectroscopies combined with isotopic tracer studies. Catalysts will be prepared by exploring novel concepts and synthesis methodologies leading to well-dispersed highly-carbided Fe catalysts. **(BYU)**

3. Task 3: Use DFT calculations to determine reaction thermochemistry and kinetics for key elementary steps in Tasks 1 and 2 including propagation and termination steps and steps involving reactive intermediates such as hydrogenation of CH_2. Investigate effects of surface/subsurface O and C, at various concentrations, on the reactivity of Fe surfaces. Determine effects of promoter type and concentration, coverage of surface/subsurface carbon species, and surface defects on the kinetic/thermodynamic parameters for key steps. **(UW)**

4. Task 4: Obtain a statistical set of rate and selectivity data on $Fe/K_2O/Cu$ supported on SiO_2 or Al_2O_3 (and structurally promoted with ZnO or ZrO_2) catalysts over a relevant range of reaction temperatures, reactant compositions, and H_2/CO ratios and use these data to validate the microkinetic model. **(BYU and UW)**

5. Task 5: Build collaborative relationships with other research groups and with companies and develop proposals for funding the continuation of the proposed work and its incorporation into a comprehensive catalyst particle/reactor/process model. **(BYU and UW)**

IV. DELIVERABLES

1. A microkinetic model that will enable prediction of catalyst activity and hydrocarbon selectivities over a range of temperatures, pressures, H_2/CO ratio, and as a function of promoter type and of the surface/subsurface carbon coverage. The model is expected to address the molecular principles governing the relative rates of chain growth versus termination on iron FTS catalysts, thereby providing a basis for maximizing desirable products.

2. First-Principles DFT calculations of binding energies, reaction barriers, and pre-exponential factors estimates for key elementary steps in the FTS mechanism.

3. Kinetic parameters for key elementary steps including CO and H_2 adsorption/dissociation, hydrogenation of various carbon containing species, olefin adsorption on unpromoted and promoted $Fe/K_2O/Cu$, under high pressure conditions using TPD and temperature-programmed reaction spectroscopies combined with isotopic tracer studies.

4. A statistical set of rate and selectivity data on $Fe/K_2O/Cu$ catalysts over a relevant range of reaction temperatures, reactant compositions, and H_2/CO ratios that can be used to validate mechanistic models.

Executive Summary

The principal objective of this research is to develop and validate a detailed microkinetic submodel which describes the rates of the important elementary steps that occur on the surface of an iron catalyst during FTS. The model will incorporate the effects of potassium oxide, a Pt promoter, and subsurface carbon species on the important elementary steps.

Much of the effort during this first year focused on (1) searching/summarizing published FTS mechanistic and kinetic studies of FTS reactions on iron catalysts; (2) construction of mass spectrometer-TPD and Berty CSTR reactor systems; (3) preparation and characterization of unsupported iron and alumina-supported iron catalysts at various iron loadings; (4) determination of thermochemcial and kinetic parameters such as binding energies of reactive intermediates, heat of reaction and activation energy, frequency factor of FTS elementary steps on specifically chosen model Fe surfaces.

Literature describing mechanistic and kinetic studies of Fischer-Tropsch synthesis on iron catalysts was searched, studied and compiled in a review; updating of this comprehensive, critical review is in progress and will continue for the next six months; it will be submitted for publication towards the end of the coming year. The review includes compilations of kinetic data for elementary steps, mechanistic schemes, and global rate equations for FTS on iron catalysts. A plausible FTS mechanism has been adopted that will serve as a foundation for development of the microkinetic model and as a guide for experimental and computational studies. Mechanistic steps for which data are lacking or for which there is uncertainty regarding reaction paths are being identified and will become high priorities in our investigation.

Work during this past year produced (1) substantial improvements in our equipment and methods for studying CO and H_2 adsorption properties, mechanisms and kinetics of elementary surface reactions, and global kinetics of these model iron catalyst systems, and (2) evaluation of preparation methods, support design, and supported iron catalyst design that has enabled our ongoing development of a suite of six active, selective, stable iron/alumina catalysts having a range of iron contents for use in our mechanistic and kinetics studies.

Methods for preparation of alumina-supported iron catalysts suitable for kinetic and mechanistic studies in FTS process were investigated. Three unsupported iron catalysts and three alumina-supported iron catalysts were prepared by non-aqueous, evaporative deposition (NED), aqueous impregnation (AI), and co-precipitation methods. These catalysts, covering a wide range of dispersions and metal loadings, are well-reduced and relatively thermally stable up to 500-600°C in H_2, thus ideal for kinetic and mechanistic studies.

Several kinds of experiments were undertaken in the characterization of the catalysts prepared thus far, including Thermogravimetric Analysis-Temperature Programmed Reduction

(TGA-TPR), BET surface area measurements, H_2 and CO chemisorptions, X-ray Diffraction (XRD) analysis, and Transmission Electron Microscopy (TEM).

A 10 wt% Fe alumina-supported iron catalyst prepared by the NED method and reduced at 500ºC for 12 h has a BET surface of 138 m^2/g and pore diameter of 9.5 nm. TGA-TPR experiments reveal that 10 wt% and 20 wt% Fe/Al_2O_3 catalysts prepared by NED method are more easily reduced, i.e., have a higher extent of reduction than 10 Fe/Al_2O_3 prepared by AI method. Furthermore, iron crystallite diameters estimated by H_2 chemisorption, XRD, and TEM measurements provide evidence that iron metal dispersions of Fe/Al_2O_3 catalysts prepared by the NED method are higher. CO chemisorption uptakes of Fe/Al_2O_3 are unexpectedly high, e.g., CO/Fe ratios are about 1.0 and 0.38 for 10 and 20 % Fe/Al_2O_3 catalysts, respectively. These results suggest that significant CO uptake occurs on the support as well as on the metal; thus, a correction for the support contribution must be determined. On the other hand, the CO/Fe ratio is only 0.062 for unsupported iron catalyst, consistent with a dispersion of 6-10% depending upon the stoichiometry of CO adsorption.

In the coming year, adsorption/desorption properties, rates of elementary steps, and global reaction rates will be measured for these catalysts, with and without promoters, providing a database for understanding effects of dispersion, metal loading, and support on elementary kinetic parameters and for validation of computational models that incorporate effects of surface structure and promoters.

Using state-of-the-art periodic DFT methods, we analyzed the thermochemistry and kinetics of the various FTS elementary reaction steps. This involved determining the binding energies and entropies of adsorbed FTS intermediates. Furthermore, we determined the activation energies and the frequency factors associated with these elementary steps. These parameters were determined on Fe(110), the most close-packed surface for Fe, and on a Fe(110) surface with ¼ ML subsurface carbon. These studies provided useful insights for the effect of subsurface carbon on the reactivity of Fe catalysts and has generated a reliable initial set of parameters which can be used for building a comprehensive microkinetic model. The DFT-based microkinetic model is expected to improve our understanding of the FTS mechanism, by yielding information such as surface coverage of various species, reaction orders, apparent activation energy, rate-determining step, and dominant reaction paths as a function of reaction conditions. Developing this model and deriving this information out of that is going to be at the center of our activities for the coming year. In parallel, we are advancing our understanding of FTS elementary steps in the presence of surface Pt, which is a fine promoter of FTS. Our preliminary DFT work in that topic appears to be yielding some fundamental insights which may prove to be key for explaining the increased selectivity of Pt-promoted Fe-based catalysts towards higher hydrocarbons.

Experimental Procedures

A. Preparation of Alumina Binder and Supported Fe Catalysts

1. Preparation of stabilized γ-Al$_2$O$_3$

The purpose of this procedure is to produce a support of exceptional hydrothermal stability (since FTS is conducted at high partial pressures of product steam). This ensures that our supported catalysts will be stable during our mechanistic and kinetic studies. Two approaches were used to improve the hydrothermal stability of a γ-Al$_2$O$_3$ support. (1) γ-Al$_2$O$_3$ (Alumina 200L3, Sasol) was stabilized by calcination at 650ºC for 6 h in air (samples is denoted as Al-1); (2) γ-Al$_2$O$_3$ was stabilized by addition of La oxide (about 6 wt%) using a specific adsorption method (sample is denoted as AlLa-1). In Approach 2, 20 g of alumina (Catapal A) material was suspended in 750 ml of demineralized water in a beaker equipped with Ar gas flow. The pH of the suspension was adjusted to 5 by addition of concentrated nitric acid. EDTA (3.507 g) was dissolved in 90 ml of demineralized water by increasing the pH from 3 to 5 with the addition of concentrated ammonia. An equimolar amount of La(NO$_3$)$_3$·6H$_2$O was dissolved in 18 ml of demineralized water and slowly added to the EDTA solution. The pH of this solution was also adjusted to 5. The [La(EDTA)]$^-$ solution was added to the vigorously stirred suspension of alumina, and the pH was kept constant by the addition of diluted nitric acid. The temperature of the suspension was 25ºC. After 2 h, since most of the La nitrate had adsorbed to the alumina, the suspension was filtered, and washed with demineralized water. The lanthanum concentration in the filtrate was determined by ICP. The loaded support was dried at 60ºC overnight, then, calcination at 900ºC for 5 h while heating at around 5ºC/min. Finally, the sample was steam treated at 850ºC for 12 h with the He/steam ratio of 1:1.

2. Preparation of 1 wt% Al$_2$O$_3$ / 99 wt% Fe Catalyst

Fe(NO$_3$)$_3$·9H$_2$O(AR) and Al(NO$_3$)$_3$·9H$_2$O(AR) were mixed to the desired ratio and were dissolved to obtain an aqueous solution with total cation concentrations of 1 M. NH$_4$OH(AR) was dissolved in demineralized water to form another aqueous solution with the appropriate amount calculated according to the relation [NH$_4$OH] = 3.2[M^{3+}]. The NH$_4$OH solution was added dropwise to the solution of Fe(NO$_3$)$_3$ and Al(NO$_3$)$_3$ solution at 70ºC while stirring over an interval of 2 h, during which time a brown precipitate was formed. The pH of the slurry was controlled in the range of 8 to 9. After precipitation, the slurry was stirred for another 30 min at 70ºC. The precipitate was filtered, washed with demineralized water, and dried at 110ºC overnight. The sample is designated as 99FeA

3. Preparation of Al$_2$O$_3$-Promoted Iron Catalysts with 1 wt% K, or 1 wt% Pt Promoters

Samples of washed and dried 99FeA were impregnated with K$_2$CO$_3$ or H$_2$PtCl$_4$ solutions, to produce catalysts containing 1 wt% K or 1 wt% Pt, respectively. The samples were dried at 110ºC overnight. These two samples are designated as 99FeAK and 99FeAPt, respectively.

4. Preparation of 10 wt% Fe/Al₂O₃ Catalysts

a. 10 wt% Fe/Al$_2$O$_3$ Catalyst with Aqueous Solution

This sample was prepared by an incipient wetness impregnation method. A pre-measured amount of iron nitrate was dissolved in demineralized water. The solution was added to the alumina support. The sample was set aside at RT for 10 h after which the sample was dried at 110ºC overnight. The sample is denoted 10FeA-W.

b. 10 wt% Fe/Al$_2$O$_3$ Catalyst with Acetone/Ethanol Solution

Fe(NO$_3$)$_3$·9H$_2$O was added to a flask, which was immersed into a water bath at a temperature of 52ºC and connected to a vacuum pump. The melted Fe(NO$_3$)$_3$·9H$_2$O salt was evacuated for 24 h. The final weight of iron nitrate was about 70.25% of the starting weight. While the iron nitrate was still liquid, 10 ml ethanol and 10 ml acetone were added to dissolve it. Alumina powder (Al-1) previously calcined at 650ºC for 6 h, was added to the solution and the sample was stirred well by shaking. The sample was put aside at RT until the ethanol/acetone had evaporated. The sample was then dried at 110ºC overnight and is denoted as 10FeA-A/E.

5. Preparation of 20 wt% Fe/Al₂O₃ Catalysts

A two-step impregnation (10 wt% per step) was used. Fe(NO$_3$)$_3$·9H$_2$O was treated and dissolved in acetone/ethanol as in Procedure 4b. La-alumina powder, AlLa-1, was added to the solution and the sample was stirred by shaking. Ar gas was bubbled through the solution until the ethanol/acetone had evaporated. The sample was dried at 60ºC overnight, further dried at 110ºC for another 12 h, and calcined at 300ºC for 6 h with a temperature ramp of 1ºC/min. The second impregnation treatment was repeated to reach an iron loading of 20 wt%. The sample is denoted as 20FeA-A/E.

B. Characterization of Supports and Fe Catalysts

1. BET measurements

BET surface area, pore volume, pore size, and average pore size distribution of supports and catalysts were obtained from full-range N$_2$ sorption isotherms using an adsorption surface area Tristar analyzer (Micromeritics).

2. TGA-TPR, CO adsorption measurements

Reducibility behavior measured by temperature-programmed reduction (TPR) and CO adsorption uptakes were determined by TGA (Perkin Elmer TGA7 Thermogravimetric Analyzer). TPR runs were conducted in 10% H$_2$/He at a ramping rate of 5ºC/min from RT to 850ºC. TPR curves were obtained by differentiating TGA weight loss curves. CO adsorption measurements were conducted following reduction (the experimental procedure will be explained in the Results and Discussion section).

3. Bulk reduction treatment

Catalyst samples were pre-reduced in a quartz or stainless-steel reactor placed in a temperature-programmed 3-zone furnace. Fe catalysts were calcined in air at 300ºC for 6 h at a heating ramp of 1ºC/min, and then purged in He for 30 min. After purging, 10% H_2 in He was introduced and temperature was increased from 300ºC to 500ºC at a heating ramp of 1ºC/min with a hold for 12 h at 500ºC.

4. H_2 Chemisorption Measurements

H_2 chemisorption measurements were conducted in flow chemisorption system with TCD detector. Unreduced and pre-reduced (in bulk) samples were reduced at 300ºC for 16 h and 6 h, respectively. Previously unreduced samples were calcined at 200ºC in argon for 3 h before reduction. After H_2 reduction, each sample was purged in Ar for 30 min at 300ºC then cooled to 100ºC; pure H_2 was introduced to the sample (at 100ºC) and the sample was soaked for 45 min. The sample was then cooled in H_2 with a dry ice/acetone bath to –84ºC and purged in Ar for 30 min to remove physically adsorbed H_2; it was then heated to 500ºC at 15ºC/min with a hold for 3 h at 500ºC. The H_2 uptake in this process was determined from the TCD detector area.

5. XRD measurements

Phases present in the catalysts and estimates of crystallite diameters were determined by X-ray diffraction (XRD) using the Scintag XDS2000 diffractometer equipped with a Cu target and graphite monochromator.

6. TEM images

TEM measurements were performed on a high-resolution Tecnai F30 TEM with highest magnification of 800,000. The sample powder was dissolved in methanol and mounted on the TEM grid.

C. Construction of Mass-Spectroscopy TPD and Berty CSTR Reactor Systems

A Mass-Spectroscopy/TPD system was built for conducting mechanistic studies, including studies of CO adsorption, dissociation, and surface intermediates during FTS reaction using transient isotopic tracing. A flow-schematic and photo of the system are shown in Figs. 1 and 2. A Berty CSTR reactor system was also constructed to study reaction kinetics of FTS on supported iron. A photo is shown in Fig. 3. Both systems use state-of-the-art (Labview) computer control, gas purification and metering (with mass flow controllers), and gas analytical systems (packed-bed and capillary GC is used for the Berty system analysis). Details of the equipment design and operation are available from the PI (bartc@byu.edu).
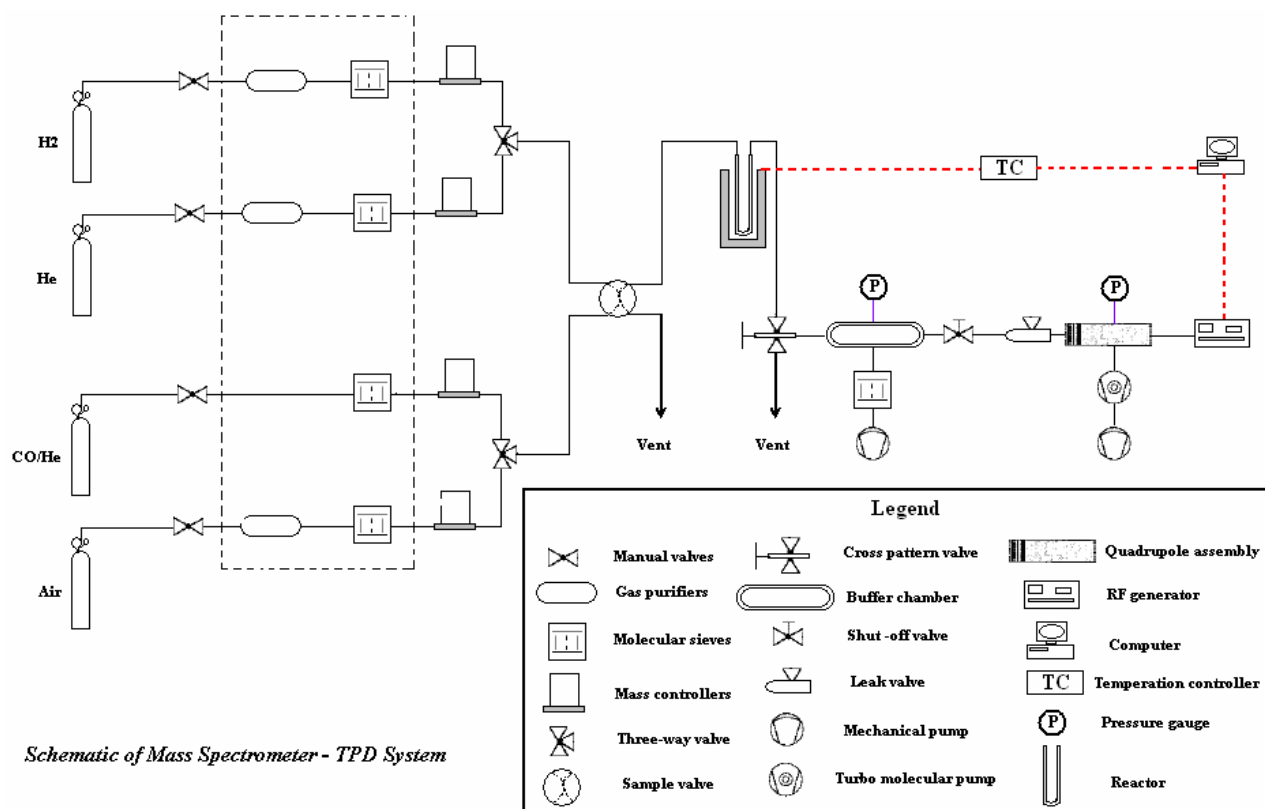
Fig. 1 Schematic of Mass Spectroscopy-TPD System

Fig. 2. Mass Spectroscopy-TPD System

Fig. 3. Berty CSTR Reactor

Theoretical Methods

All calculations are performed using DACAPO. Adsorption is allowed on only one of the two surfaces of the slab and the electrostatic potential is adjusted accordingly. Calculations were performed spin-polarized. The Fe(110) surface is modeled by a (2×2) unit cell, corresponding ,to a ¼ ML coverage for all the adsorbates. In order to investigate the effects of surface Pt and subsurface C, we have adsorbed ¼ ML Pt on the surface or ¼ ML C in subsurface. Since the Fe(110) surface is rather open, relaxation has a significant effect on the adsorption properties of various species; thus Fe is modeled using a four layer slab with the top two layers relaxed. Kohn-Sham one-electron valence states are expanded in a basis of plane waves with kinetic energy below 25 Ry. The exchange-correlation energy and potential are described by the generalized gradient approximation (GGA-PW91); the ionic cores are described by ultrasoft pseudopotentials. The surface Brillouin zone is sampled with a 4x4x1 k point set. The calculated equilibrium PW91 lattice constant for bulk Fe is $a = 2.85$ Å, in good agreement with the experimental value of 2.87 Å.

Results and Discussion based on Experiments

A. Preparation of Catalysts

Data in Table 1 include preparation conditions, BET surface areas and average pores diameters of supports and Fe catalysts. In the preparation of the alumina supported Fe catalysts, both Al-1 and AlLa-1 supports were precalcined at high temperature (650ºC and 900ºC) to substantially reduce hydroxyl group concentrations on the alumina surface. It is expected that reduction of hydroxyl group concentrations and impregnation using organic solvents enable a much higher extent of reduction of iron on these supports. Using partially dehydrated $Fe(NO_3)_3 \cdot 9H_2O$ salts at 52ºC also contributes to this objective.

Table 1. Summary of Physical Properties of Supports and Catalysts

Samples	Loadings	Codes	Calcination Temperature (ºC)	Time (h)	S_{BET} (m²/g)	Ave. Pore Diameter (nm)
			Supports			
γ-Al₂O₃		Al-1	650	6		
La/γ-Al₂O₃	6.13 wt% La₂O₃/Al₂O₃	AlLa-1	900	5	135	7.5
		AlLa-2	Steam, 850	12	73	9.1
			Catalysts			
Fe-1 wt% Al₂O₃		99FeA	110	12		
			300	6	59	10.4
			500 reduction	12	12	52.1
Fe-1 wt% Al₂O₃-1 wt% K		99FeAK	110	12		
Fe-1 wt% Al₂O₃-1 wt% Pt		99FeAPt	110	12		
10 wt% Fe/Al₂O₃	10 wt%	10FeA-W	110	12		
			300	6	182	8.0
			500 reduction	12	164	7.9
10 wt% Fe/Al-1	10 wt%	10FeA-A/E	110	12		
			300	6	166	9.1
			500 reduction	12	138	9.5
20 wt% Fe/AlLa-1	20 wt%	20FeA-A/E	60~110	24		
			300	6	156	7.7
			500 reduction	12	112	8.1

B. BET Surface Area and Pore Diameter of Supports

The goal of steam-treating the calcined lanthanum modified alumina support was to increase the average pore diameter to the range of 10-15 nm, which is ideal for FT catalysts. The surface area of lanthanum modified support calcined at 900ºC for 5 h (AlLa-1) of 135 m^2/g is ideal for FTS; however, the average pore diameter of 7.5 nm is undesirably low (see Table 1). After steam treatment at 850ºC for 12 h (AlLa-2), the average pore diameter increased about 21% to 9.1 nm while the surface area decreased almost 50% to 73 m^2/g. The decrease of surface area after steam treatment is larger than expected, while the increase in pore diameter is lower than expected. This is probably a function of the starting material (a relatively stable gamma alumina). While these supports could be used in preparing supported Fe catalysts for mechanistic and kinetic studies, we have recently found that commercial aluminas of larger pore size are available which would probably make for better starting materials.

The surface area of 10FeA-W prepared by aqueous impregnation is 182 m^2/g for the calcined sample and 164 m^2/g for the reduced sample (Table 1). Both values are larger than surface areas of 10FeA-A/E and 20FeA-A/E samples prepared by evaporative deposition in acetone/ethanol. This observation is reasonable given that the alumina supports for 10FeA-A/E and 20FeA-A/E samples were pre-calcined before their use in preparation of the iron catalysts. The surface area and average pore size of 10FeA-A/E and 20FeA-A/E samples are nevertheless suitable for FTS.

C. TGA-TPR Measurements

99FeA Catalyst

TPHe measurement

The TPHe-TGA decomposition pattern of dried samples in helium is shown in Fig. 4. The differentiated curve is characterized by overlapping peaks around 80-120ºC, 150-300ºC, and 320-400ºC. The peak at 80-100ºC is easily assigned to removal of physically adsorbed water. Other peaks starting at 150-300ºC are probably due to decomposition of iron hydroxide, Fe(OH)$_3$, to α-FeO(OH) and Fe$_2$O$_3$. The third peak between 320-400ºC is probably due to decomposition of remained α-FeO(OH) to Fe$_2$O$_3$ [3].

TGA-TPR measurement by H$_2$

The TGA-TPR pattern for direct reduction of dried samples in hydrogen (no calcination) is shown in Fig. 5. As in the TPHe, the peaks around 100 and 400ºC are attributed to water removal and decomposition of iron hydroxides. However, the peaks at about 267 and 286ºC may be due to the reduction of Fe$_2$O$_3$ to Fe$_3$O$_4$ [4-6]. In fact, some Fe$_2$O$_3$ is visible during the precipitation process [6]:

$$3Fe_2O_3 + H_2 \rightarrow 2Fe_3O_4 + H_2O \tag{1}$$

The peak with a maximum at 503ºC is due to a second reduction step from Fe$_3$O$_4$ to the metallic iron [4,6]:

$$Fe_3O_4 + 4H_2 \rightarrow 3Fe + 4H_2O \tag{2}$$

Weight losses associated with the peak at 286ºC and the peak at 503ºC in Fig. 5 are approximately 2.4% and 20.9%, respectively. The later value is about 8 times larger than the former one consistent with the theoretical weight loss of oxygen calculated from the reduction reactions in the previous two paragraphs.
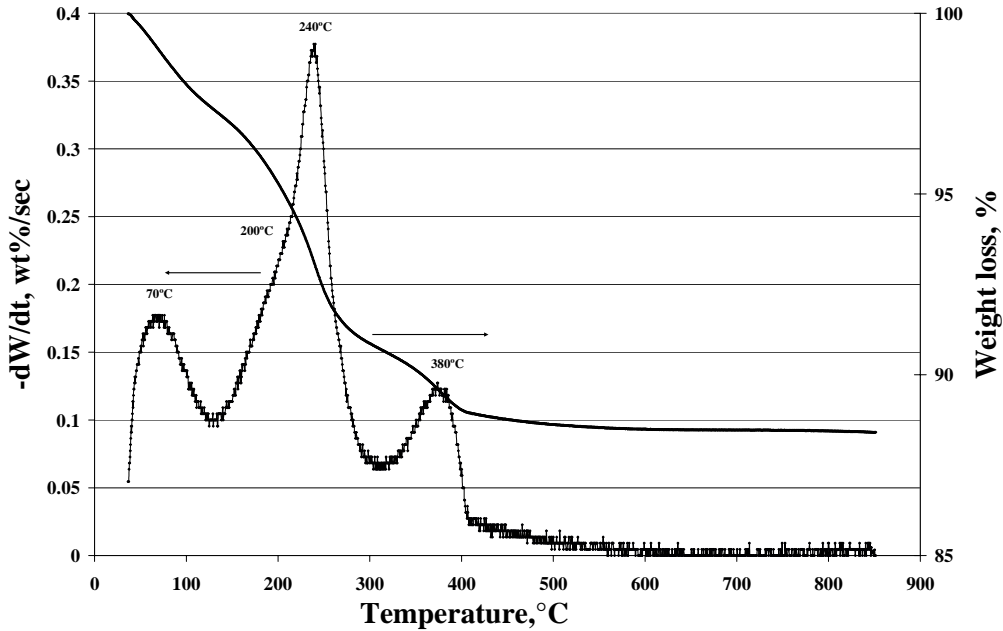

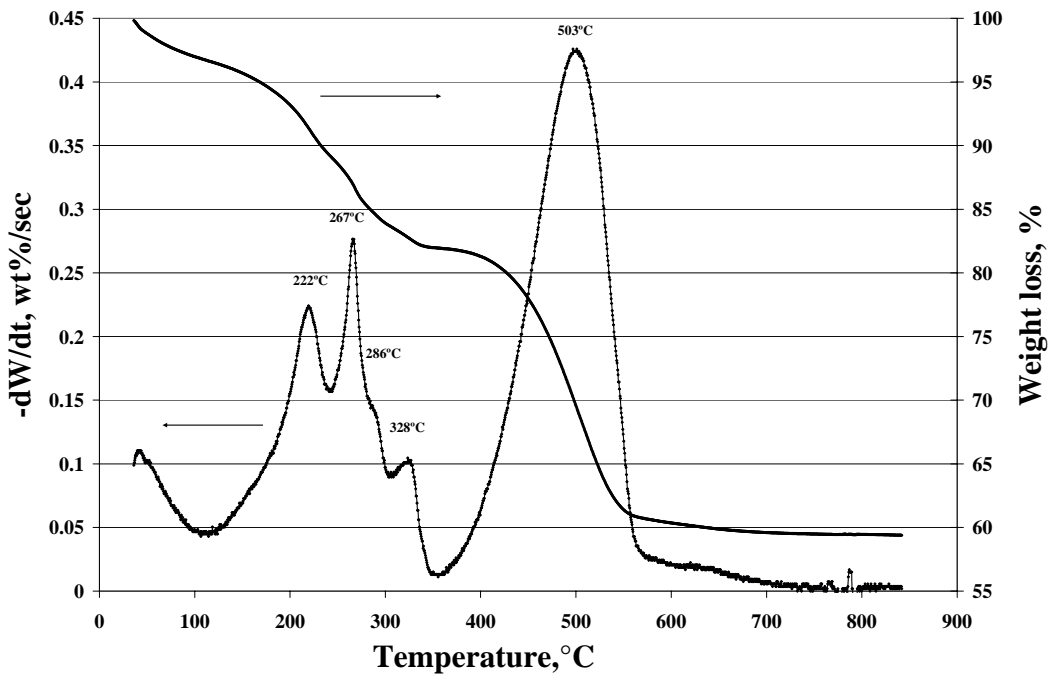**Fig. 4** TPHe/TGA spectrum of sample 99FeA

Fig. 5 TGA-TPR spectrum for H_2 reduction of sample 99FeA before calcination.

TGA-TPR measurement during reduction in CO

The TGA-TPR pattern for direct reduction of the dried 99FeA sample in CO (no calcination) is shown in Fig. 6. The profile is different from that for H_2 reduction. The peaks with maxima at 364, 468, and 605°C are probably due to the reduction of (a) Fe_3O_4 to FeO (Eqn. 3); (b) of FeO to Fe (Eqn. 4) and of Fe to Haag carbide (Eqn. 5); and (c) of FeO interacting strongly with Al_2O_3 to Fe (also Eqn. 4) and Fe to Haag carbide (also Eqn. 5) [4,7]. The negative peak at 679°C (mass

$$2Fe_3O_4 + 2CO \rightarrow 6FeO + 2CO_2 \tag{3}$$

$$FeO + CO \rightarrow Fe + CO_2 \tag{4}$$

$$15Fe + 12\,CO \rightarrow 3Fe_5C_2 + 6\,CO_2 \tag{5}$$

increase is probably due to deposition of carbon. These results need to be followed up with XRD of samples treated in CO at different temperatures.
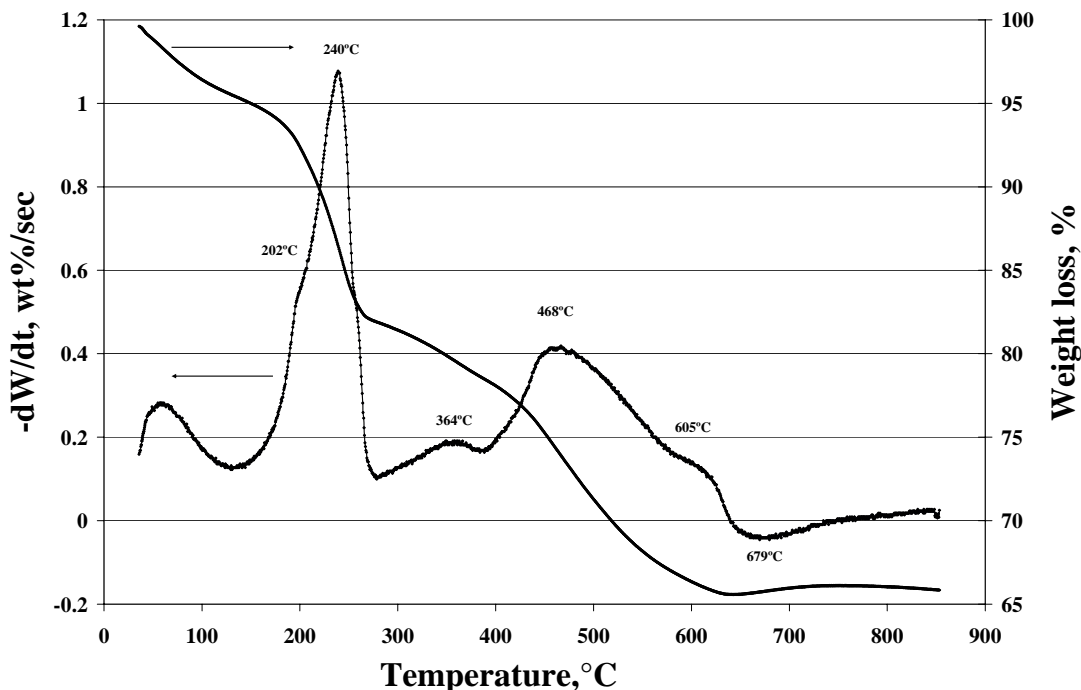

Fig. 6 TGA-TPR spectrum for CO reduction of sample 99FeA before calcination.

CO adsorption and desorption measured by TGA

CO adsorption and desorption on 99FeA sample were conducted as follows. A catalyst sample 40-50 mg was charged to the TGA pan. The sample was first reduced in 10% H_2/N_2 as follows: 1°C/min from room temperature to 120°C, hold at 120°C for 1 h, 1°C/min to 400°C, and hold at 400°C for 12 h. After reduction, H_2 flow was discontinued, while He flow was continued for 30 min at 400°C to desorb H_2. The sample was cooled to room temperature in flowing N_2. CO was introduced to the sample at room temperature by flowing 10% CO/He for 1 h. Finally, the sample was exposed to pure N_2 while temperature was increased linearly to desorb CO.

14

The procedure and the CO adsorption/desorption profile are shown in Fig. 7. The weight change in the profile was used to calculate the extent of reduction (EOR) and the amount of CO adsorption/desorption on iron samples (data in Table 2). The weight increase after introduction of CO after about 1900 min corresponds to CO adsorption on the sample. However, the weight didn't decrease during the subsequent N_2 purge during which temperature was increased stepwise to about 400ºC, indicating no desorption of CO. This result suggests that either CO is very strongly adsorbed or that during desorption it dissociated to atomic carbon which diffuses into the subsurface layers of Fe, forming a stable carbide. The extent of reduction (EOR) of the sample is high (90.6%) and the CO/α-Fe ratio of 0.062, indicates a dispersion of 6.2%--which is quite acceptable for unsupported Fe.
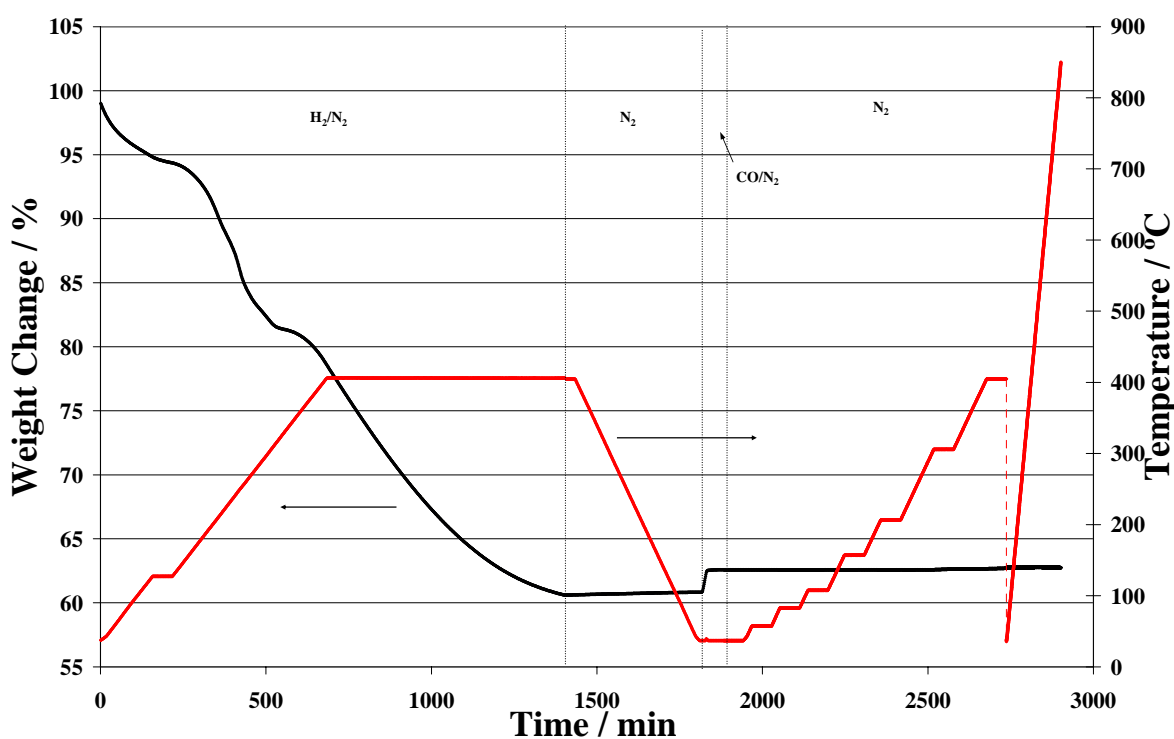

Fig. 7 CO adsorption and desorption profiles for sample 99FeA
(black line: weight change; red line: temperature program).

Table 2. Summary of EOR and CO Adsorption/desorption Results

Samples	EOR, %	CO/α-Fe (mol/mol)	CO_{des} (mol/mol Fe)
99FeA	91	0.062	None
10FeA-W	49	0.95	0.96
10FeA-A/E	60	0.94	0.94
20FeA-A/E	45	0.38	0.29

15

99FeAK Catalyst

TPHe measurement

The TPHe pattern of dried 99FeAK sample in helium is shown in Fig. 8. Two main peaks appear at 237ºC and 359ºC, similar to the peaks attributed to decomposition of iron hydroxide, $Fe(OH)_3$, to α-FeO(OH) and α-FeO(OH) to Fe_2O_3 [3] in the TPR profile of sample 99FeA in Fig. 4.
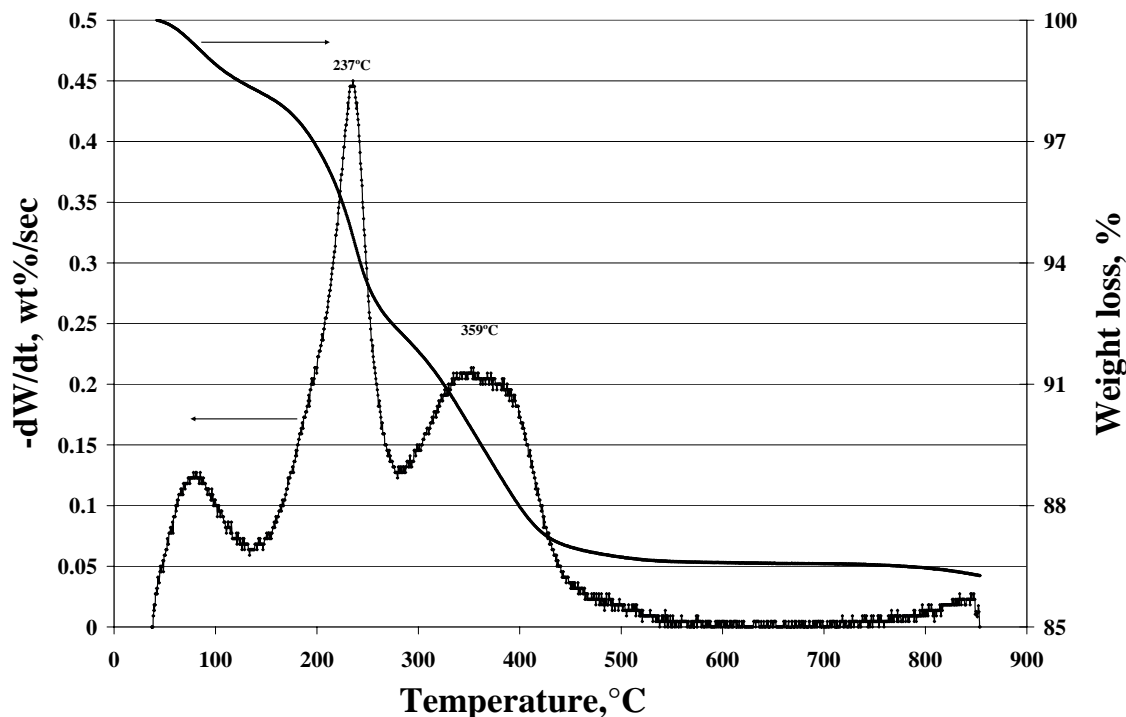

Fig. 8 TPHe/TGA spectrum of 99FeAK sample

TGA-TPR measurements by H_2

The TGA-TPR pattern of a predried 99FeAK sample in hydrogen is shown in Fig. 9. The profile is similar to that of sample 99FeA (Fig. 5) with the exception of a new peak appearing at high temperature (809ºC), which is probably due to reduction of potassium ferrite. The reduction peak for Fe_3O_4 is shifted to higher temperature (554ºC relative to 503ºC) with a small shoulder peak at 606ºC, probably due to the reduction of FeO to Fe. The +51ºC shift indicates that reduction of potassium-promoted iron is more difficult than for the unpromoted catalyst.
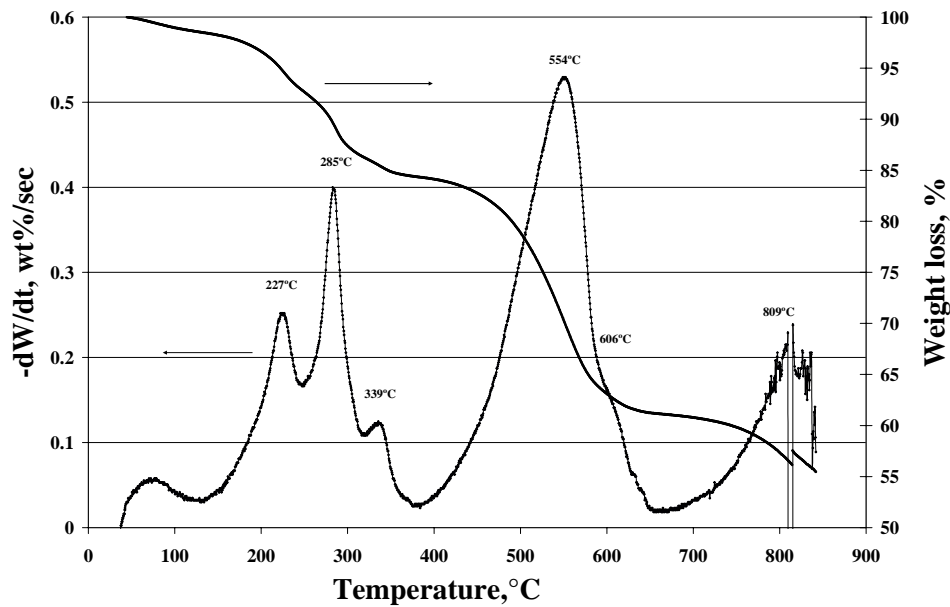
16

Fig. 9 TGA-TPR pattern by H_2 of 99FeAK sample

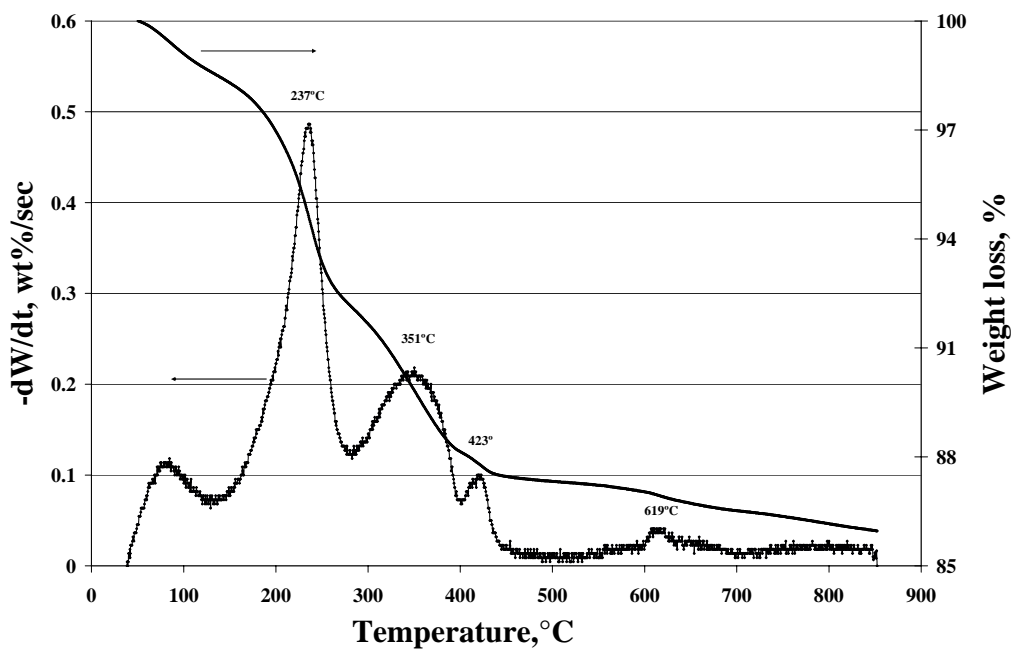### 99FeAPt Catalyst

TPHe measurement

Fig. 10 TPHe/TGA spectrum of 99FeAPt sample

The TPHe/TGA pattern of dried 99FeAPt sample in He is shown in Fig. 10. An obvious difference of this TGA pattern with those of both 99FeA and 99FeAK samples is two additional

small peaks at around 423ºC and 619ºC, which are possibly due to the Pt-catalyzed reduction of FeO_x and/orAl_2O_3 to $PtAl_x$ or PtFe.

TGA-TPR measurements by H_2

The TGA-TPR pattern of dried 99FeAPt sample in hydrogen is shown in Fig. 11. The most important differences with the corresponding spectrum for 99FeA (Fig. 5) are shifts of the peaks at 146, 237, 283, and 294°C to lower temperatures compared to unpromoted Fe. This is consistent with the expectation that Pt would assist the reduction of Fe.
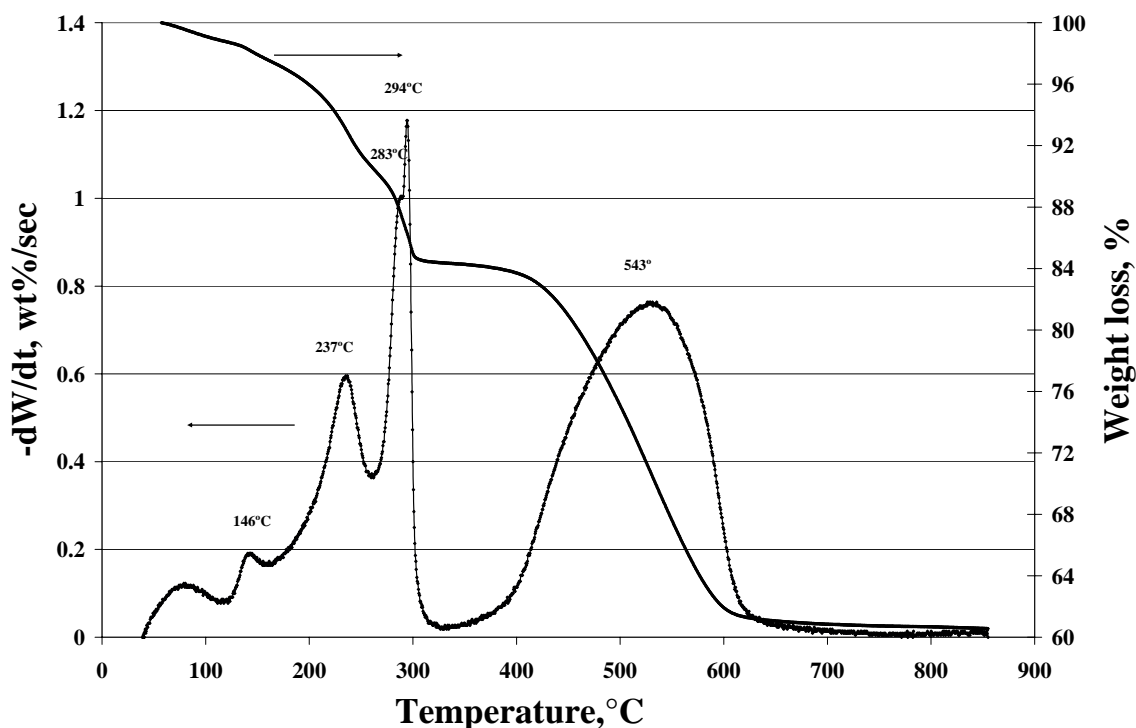

Fig. 11 TGA-TPR pattern by H_2 of 99FeAPt sample

10FeA Catalysts

TGA-TPR measurements by H_2

The decomposition of 10% Fe/Al_2O_3 (10FeA) catalysts in He is much simpler than that of 99FeA samples because the iron precursor in the 10FeA samples is iron nitrate. TGA For example the He decomposition pattern of the 10FeA-W catalyst (Fig. 12) consists of two low temperature peaks at 213 and 258ºC attributed to decomposition of iron nitrate.

Figure 13 shows the TPR patterns of three 10FeA catalyst prepared by different methods, after drying at 110ºC for 12 h. Three large peaks at 155ºC, 225ºC, and 305ºC are observed for the dried 10FeA-W sample. The peak at 155ºC is attributed on the basis of the TPHe results to the decomposition of iron nitrate. Generally, the reduction reaction proceeds in a stepwise manner:
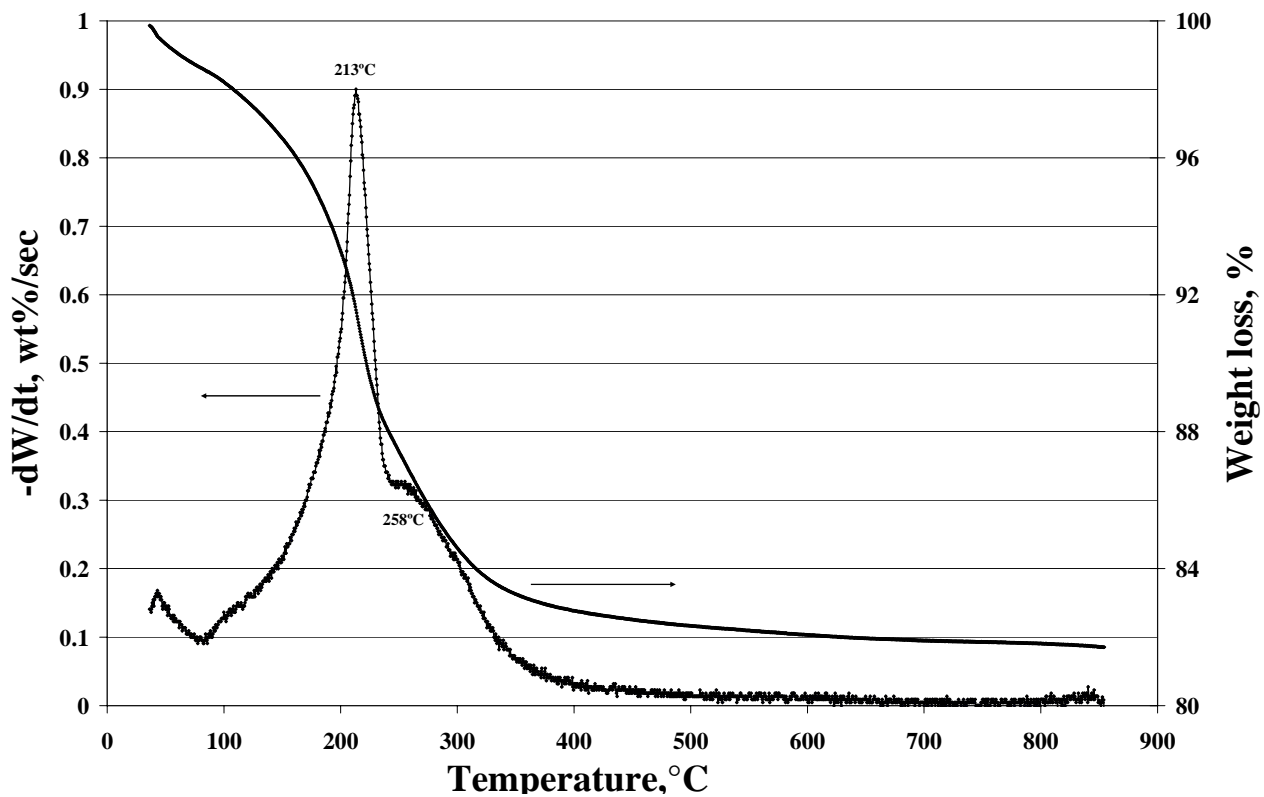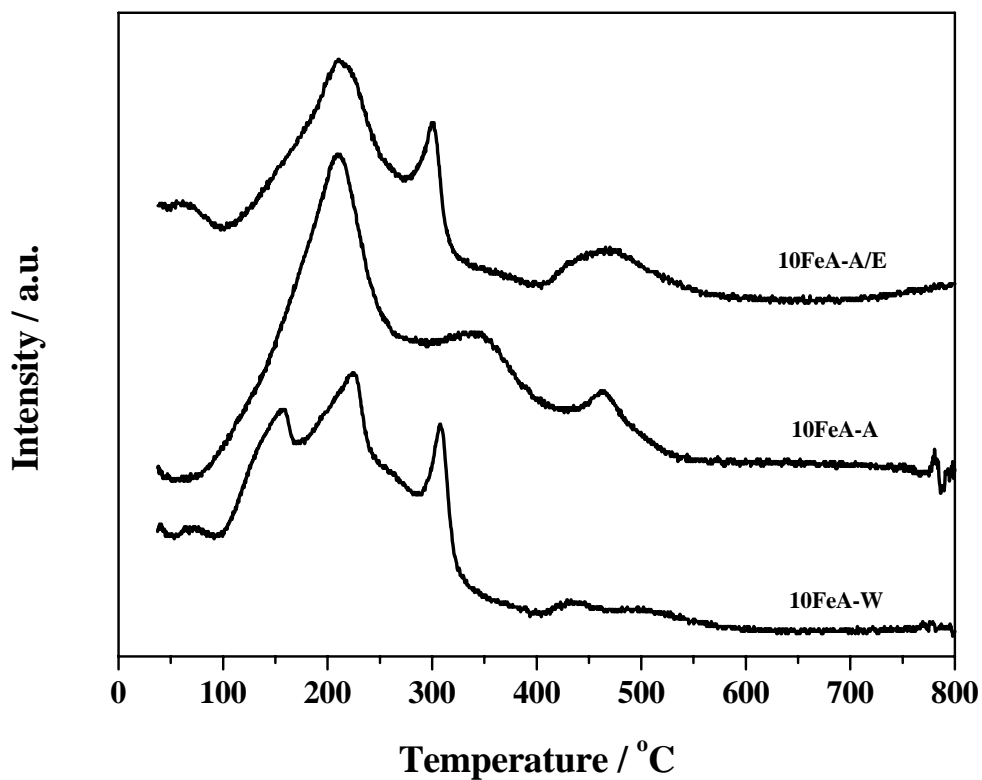
18

Fig. 12 TPHe/TGA pattern of sample 10FeA-W

Fig. 13 TPR patterns of 10FeA samples

19

α-Fe$_2$O$_3$ (hematite) $\rightarrow$ Fe$_3$O$_4$ (magnetite) $\rightarrow$ FeO (wustite) $\rightarrow$ α-Fe (iron) [4-7]. The largest TPR peak with a peak maximum at 225ºC sits on a broad envelope from about 180 to 280ºC which appears to consist of several overlapping peaks. This broad envelope is assigned on the basis of literature [4-7] and observations in this study to stepwise reduction of α-Fe$_2$O$_3$ to Fe$_3$O$_4$ to FeO. The peak at 305ºC is assigned unambiguously to the reduction of FeO to Fe, since we found that after prolonged reduction at 300ºC, about 50% of the iron was present as Fe metal. The small broad peak from 400ºC to 500ºC is assigned to the reduction to Fe metal of FeO interacting strongly with the alumina support. For the other two samples, FeA-A (acetone) and 10FeA-A/E (acetone/ethanol), three peaks are seen in their TPR patterns. The broad peak from 100 to 300ºC with a peak maximum at 215ºC is assigned to the decomposition of Fe-acetone-polymers followed by the stepwise reduction of of α-Fe$_2$O$_3$ to Fe$_3$O$_4$, and Fe$_3$O$_4$ to FeO. The peaks at 300ºC for FeA-A/E and at 340ºC for 10FeA-A are attributed to the reduction of FeO to Fe. The last peak around 450-475ºC is assigned to the reduction to Fe metal of FeO interacting strongly with the alumina support.

CO adsorption and desorption measured by TGA

CO adsorption on 10FeA catalysts was conducted at room temperature using a procedure similar to that for the 99FeA catalyst. CO desorption was conducted in He while increasing temperature in one or two steps to about 750-800ºC. The CO adsorption/desorption patterns of 10FeA-W and 10FeA-A/E catalysts are presented in Figs. 14 and 15, respectively. RT CO adsorption is fast during the initial 100-200 min for both samples, then slows down and reaches saturation at 400-500 min. The CO desorption process of these two samples is apparently exponential and significantly influenced by heating rate. The results of CO adsorption/desorption measurements are listed in Table 2 as the molar ratio of CO to α-Fe. The ratio of CO adsorption is close to 1.0 for both catalysts, suggesting CO adsorption occurs on both the support and metal, since neither catalyst is unidisperse. Thus, a correction for adsorption on the support will be necessary.
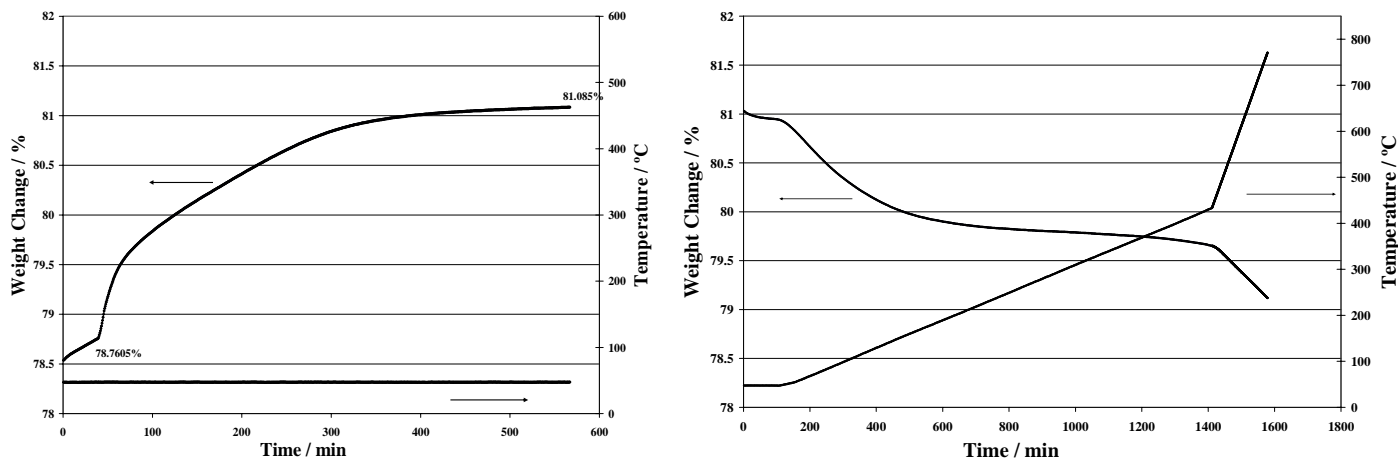

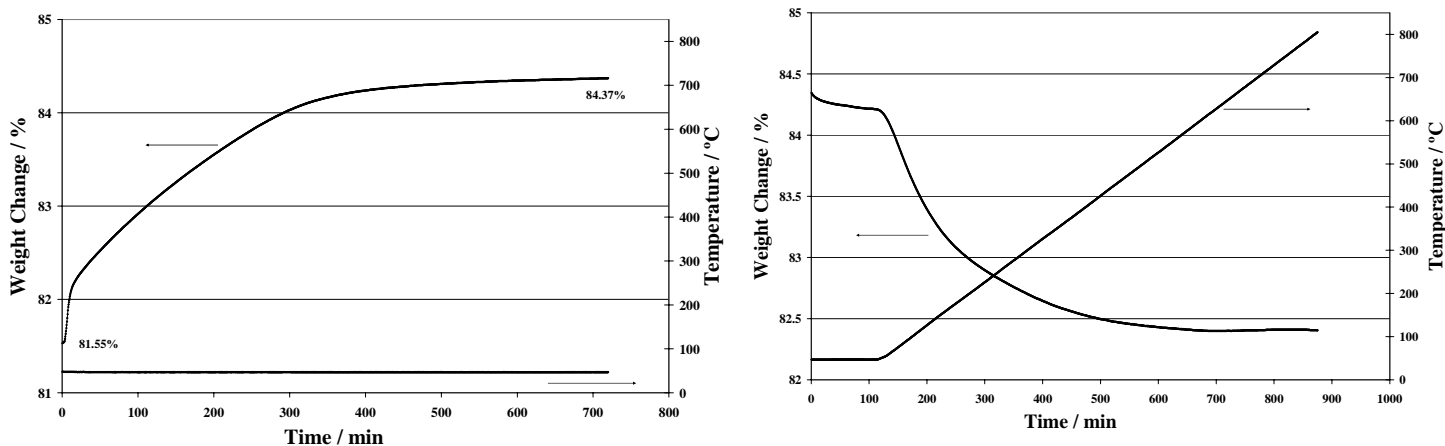**Fig. 14** CO adsorption (left) and desorption (right) patterns of 10FeA-W sample

20

Fig. 15 CO adsorption (left) and desorption (right) patterns of 10FeA-A/E sample

20FeA-A/E Catalysts

H₂-TPR

The H$_2$-TPR profile of the 20FeA-A/E catalyst calcined in air at 300ºC for 6 h is shown in Fig. 16. The overlapping peaks with a maximum at 286ºC are attributed to phase transformations of Fe$_2$O$_3$ to Fe$_3$O$_4$ and Fe$_3$O$_4$ to FeO. A shoulder at 283ºC is probably due to the reduction of FeO to Fe. Peaks at 500 and 650ºC are probably due to reduction of FeO·Al$_2$O$_3$ to Fe.
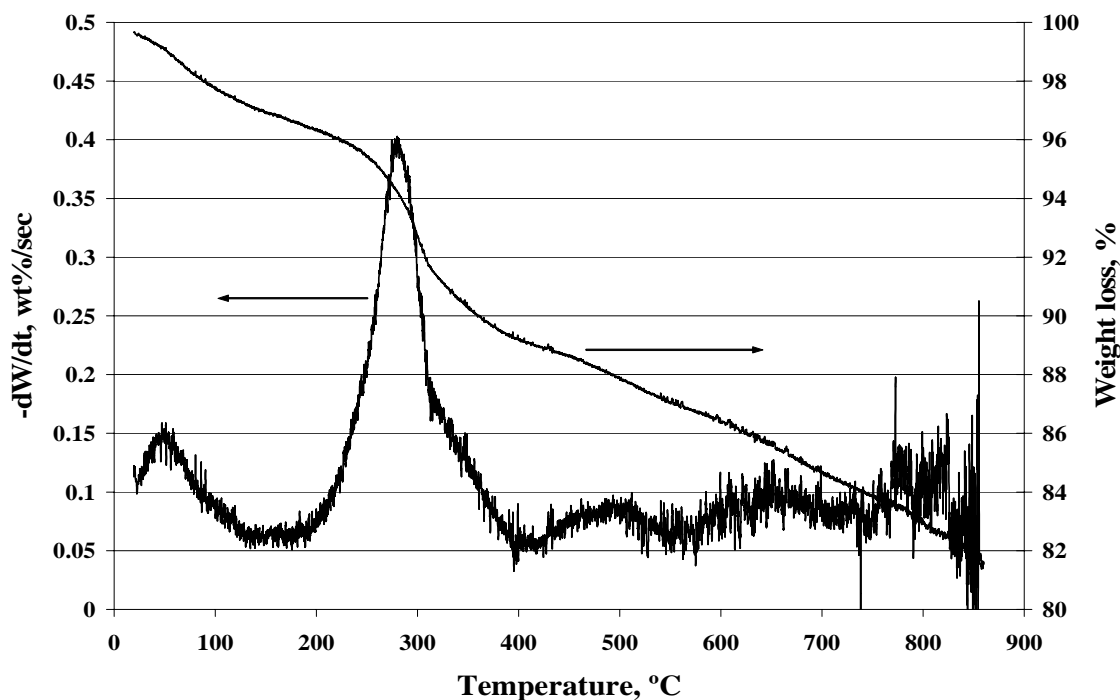

Fig. 16 TGA-TPR patterns by H$_2$ of 20FeA-A/E sample after calcination.

21

CO adsorption

CO adsorption on and desorption from the 20% Fe/Al_2O_3 catalysts (20FeA-A/E) were conducted at RT using the same procedure as for the 99FeA catalyst (see Figs. 17 and 18, respectively). The CO desorption pattern exhibits two peaks with maximum at 110ºC and 210ºC. The former is probably due to desorption of weakly bound molecular CO and the later to strongly-chemisorbed CO. CO/α-Fe ratios obtained in CO adsorption and desorption process-es of 0.38 and 0.29, respectively (Table 2) are much smaller than those of 10FeA catalysts.
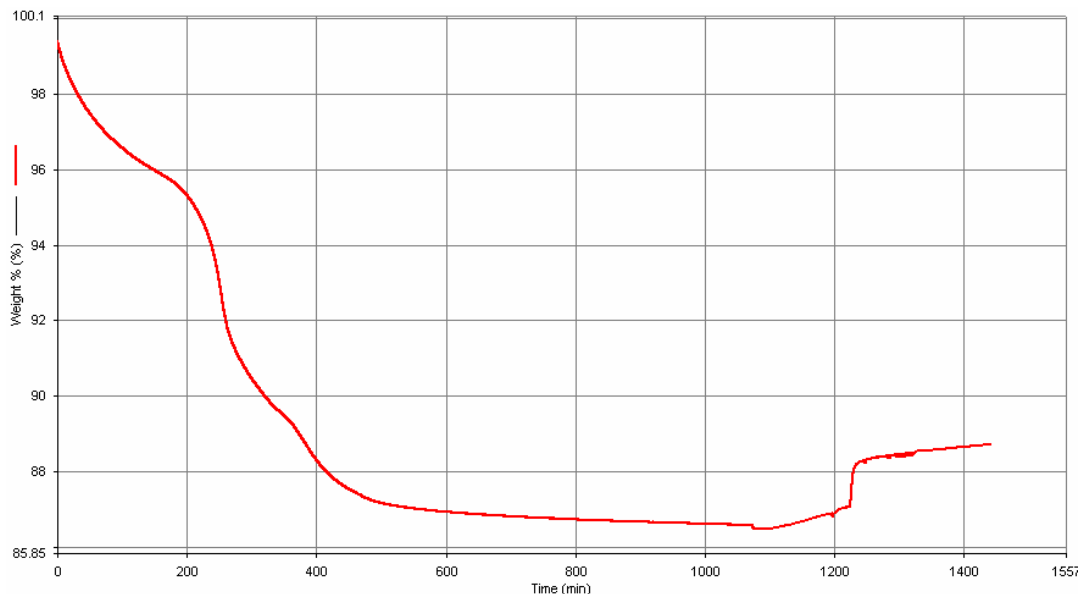

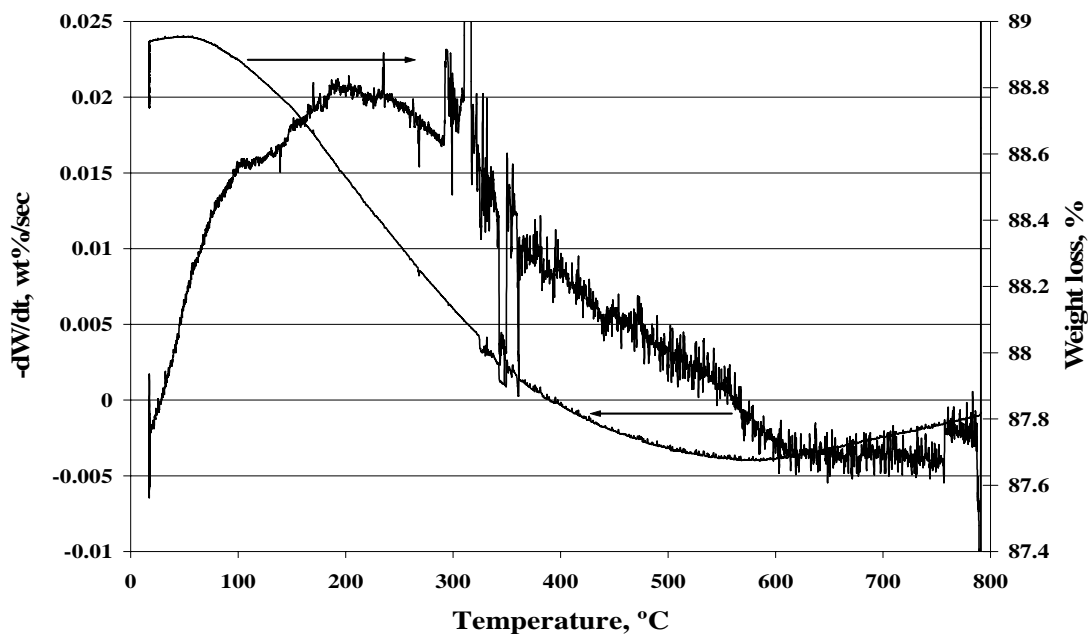**Fig. 17** CO adsorption pattern of 20FeA-A/E sample

Fig. 18 CO desorption pattern of 20FeA-A/E sample

22

D. H₂ Chemisorption Measurements

H$_2$ chemisorption uptakes of the supported iron samples are listed in Table 3. H$_2$ chemisorption uptakes for 20FeA-A/E, 10FeA-A/E, and 10FeA-W catalysts are 455, 253, and 43 μmol/g. Extents of reduction are 45, 60 and 49%, Fe dispersions catalysts are 37, 48 and 9.8%. The 37% and 48% dispersions are unusually high, and the average crystallite diameter remarkably low for the 10% and 20% Fe/alumina catalysts prepared in acetone/ethanol. The dispersion for the catalyst prepared in aqueous environment optimal for FTS, while crystallite diameters for the 10FeA-A/E catalyst of 2.6 nm and the 20FeA-A/E catalyst of 3.3 nm are too small to be stable during FTS at high conversions where water partial pressures are likely to be high enough to oxidize these crystallites of high surface energy. These high uptakes and dispersions, however, are unprecedented for supported Fe and of great interest in terms of catalyst design. As a check on these results, crystallite diameters were determined independently from XRD and TEM.

Table 3. H₂ Chemisorption Results (data are the average of 2-3 runs)

Catalysts	H$_2$ uptake [a] (μmol/g catalyst)	EOR,%	%D [b]	d(nm) [c]
10FeA-W	43	49	9.8	12.6
10FeA-A/E	253	60	47.5	2.6
20FeA-A/E	455 [d]	45	37.4	3.3

a. Catalysts calcined at 200ºC in argon for 3 h followed by H$_2$ reduction at 1ºC/min from 200ºC (after pretreatment) to 300ºC with a hold for 16 h at 300ºC, and then was run H$_2$ uptake.

b. %D = $C_2X/(100fw)$: C_2 is a constant, Fe = 1.12; X is the chemisorptive uptake; f is the fraction of active element present in the metallic state; and w is the weight fraction of the catalytic element present as either metal or oxide.

c. d = $C_1/(\%D)$: C_1 is a constant for a given catalytic phase, Fe = 123.

d. This catalyst was bulk reduced by H$_2$ at 500ºC for 12 h before measurement of H$_2$ uptake.

E. XRD Measurements

XRD measurements were conduced on all iron catalysts for both calcined and reduced samples. The XRD spectra in Fig. 19 are the diffraction patterns of the catalyst samples taken after calcination in air at 300ºC for 6 h.The peaks at 33º, 35.7º, 41º, 49.6º, 54.2º, 62.5º, and 64.2º in the diffraction pattern of 99FeA sample, shown in Fig. 19 curve D, are attributed to α-Fe$_2$O$_3$ phase. It indicates that α-Fe$_2$O$_3$ phase is formed after calcination at 300ºC, in agreement with the conclusion drawn from TPHe-TGA experiments. The diffraction patterns of three supported iron catalysts are similar with the diffraction pattern of pure alumina support, not shown in the figure, indicating there is not iron based phase formed on the surface of those samples. However, TPHe-TGA measurements reveal decomposition of iron compounds to iron oxide is finished before 300ºC. Thus, the possibility is that the portion of iron oxide on supported iron catalysts is too small to be detected by XRD technique.

The XRD patterns of the catalyst samples after reduction in H_2/He at 500ºC for 12 h are shown in Fig. 20. Two iron phases can be detected in the XRD patterns of 99FeA sample based on the characteristic diffraction peaks. The peaks at 44.5º and 65.5º are attributed to α-Fe and the other peaks are assigned to the magnetite Fe_3O_4 phase. For the supported iron catalysts, α-Fe is also observed at 44.5º. The XRD curves between 40º and 50º of alumina-supported iron catalysts are enlarged in Fig. 21. Iron crystallite sizes of supported iron catalysts were calculated by Scherrer equation:

$$D = 0.9\lambda/(\beta\cos\theta) \tag{6}$$

where D = Crystallite size;

λ = X-ray wavelength;

β = Full width at half maximum (FWHM) of the peak;

θ = Angle at FWHM.

Iron crystallite diameters are listed in Table 4 and compared with those estimated from H_2 chemisorption and TEM.
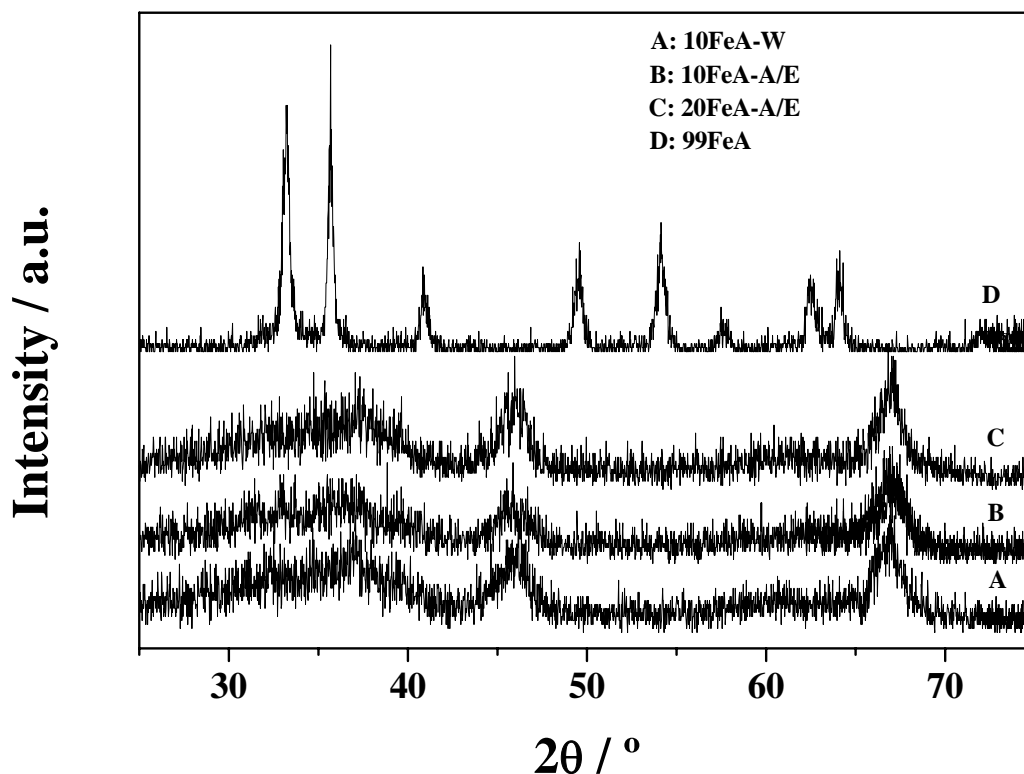

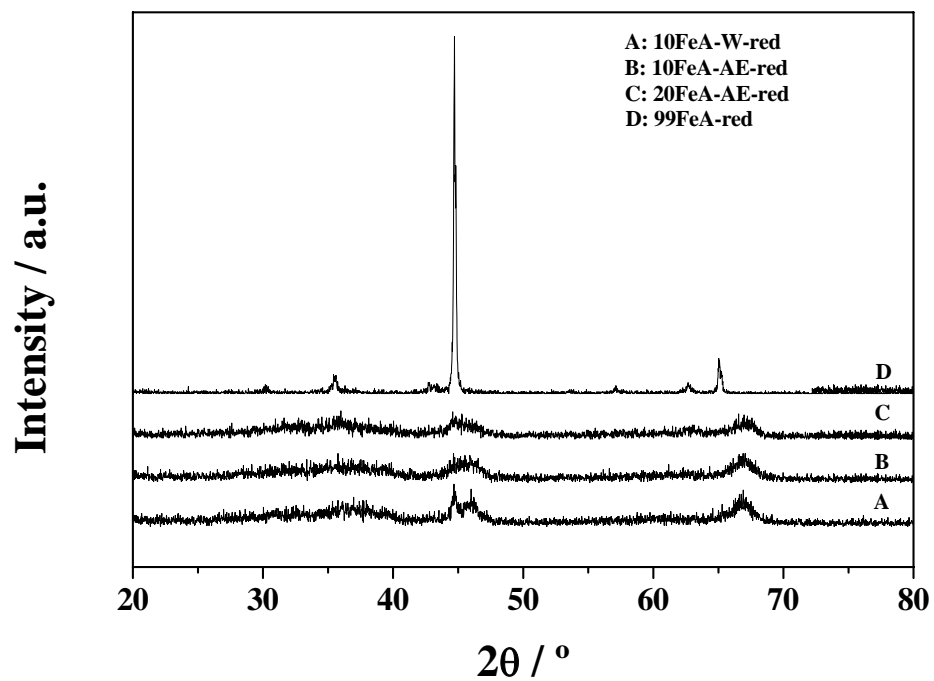**Fig. 19.** XRD Patterns of Iron Catalysts after Calcination at 300ºC for 6 h

Fig. 20. XRD Patterns of Iron Catalysts after Reduction at 500ºC for 12 h
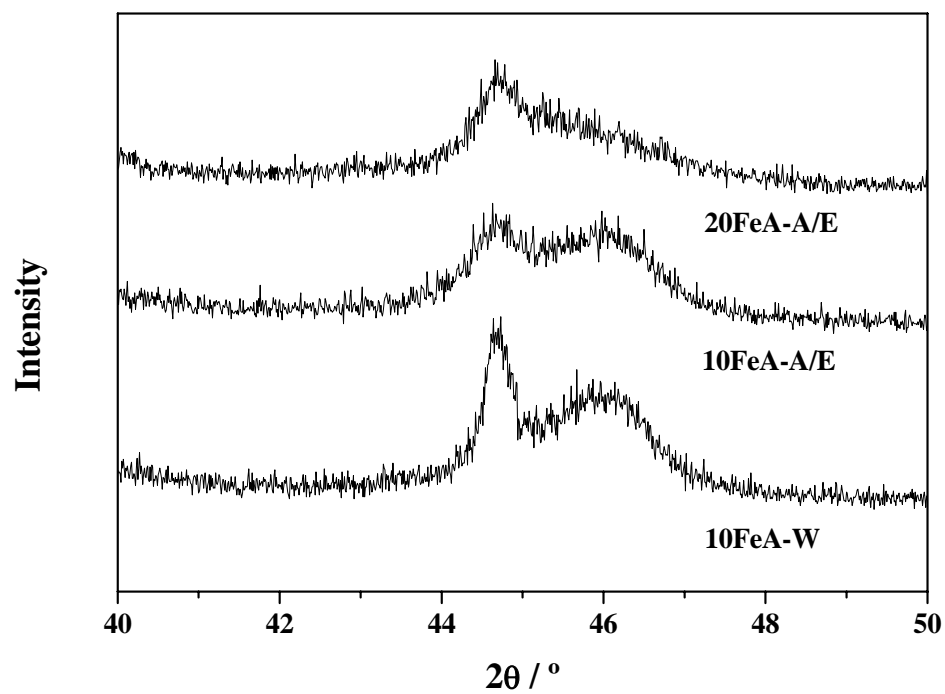

Fig. 21. XRD Patterns of Iron Catalysts in 40~50º after Reduction at 500ºC for 12 h

F. TEM Measurements

TEM was utilized to study the surface morphology and crystallite diameters of iron catalyst samples. The surface morphology includes 3-D, iron metal particle crystallites of 3-30 nm diameter; faceting is observed for the larger crystallites. TEM images of 10FeA-A/E catalyst (left) and 10FeA-W (right) are shown in Fig. 22 and of 20FeA-A/E (left) and 99FeA (right) in Fig. 23. That black spots in these images are α-Fe, was confirmed by electron diffraction (rings in corner of each figure). The iron metal sizes estimated from these images are listed in Table 4.
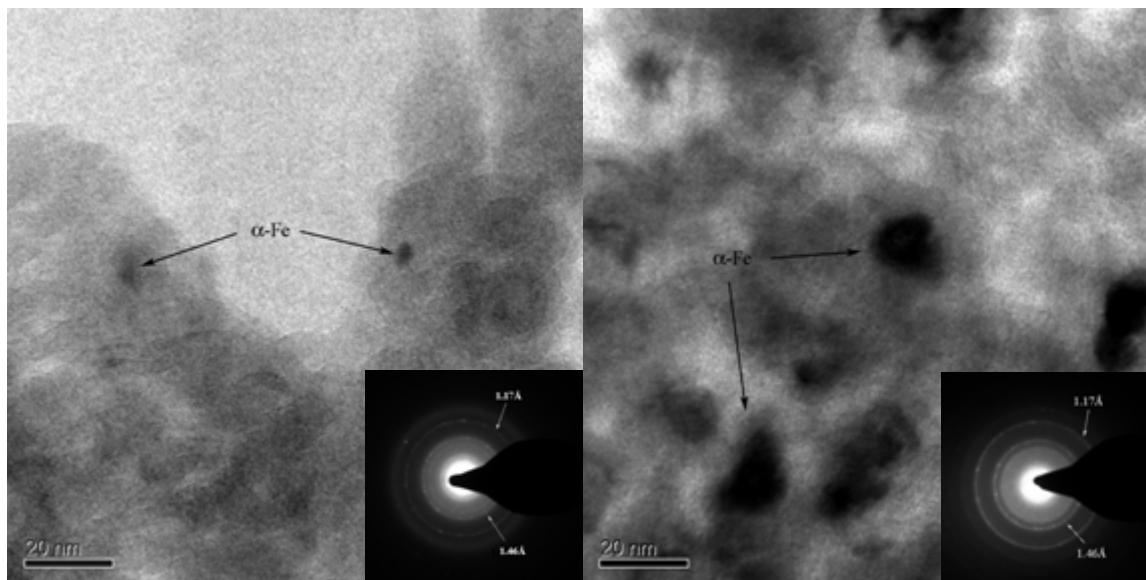

Fig. 22. TEM Images of 10FeA-A/E (left) and 10FeA-W (right) after Reduction at 500ºC for 12h
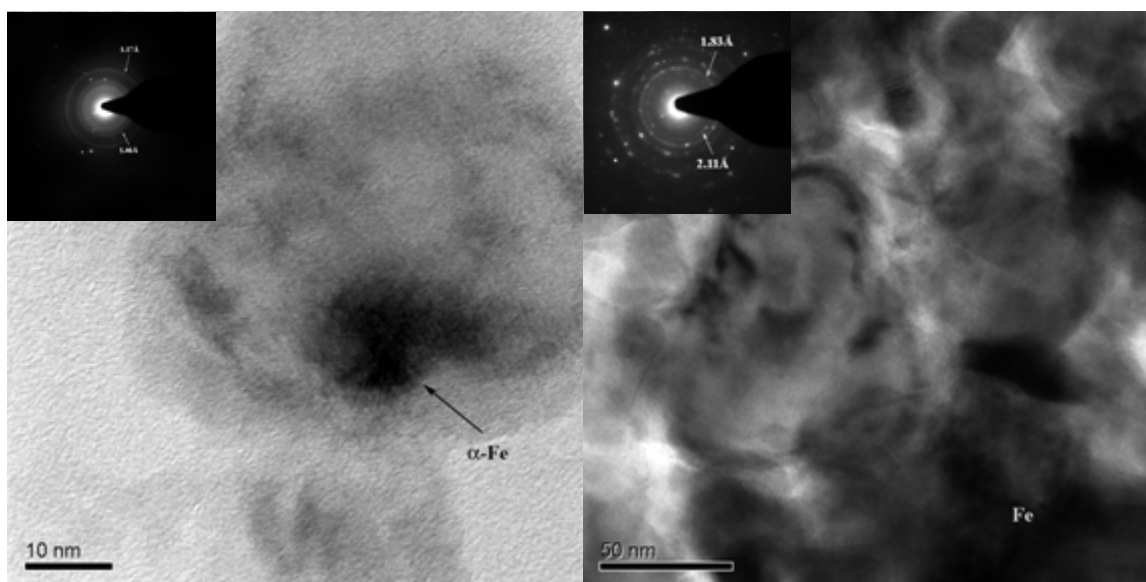

Fig. 23 TEM Images of 20FeA-A/E (left) and 99FeA (right) after Reduction at 500ºC for 12 h

Table 4 provides a comparison of iron crystallite diameters estimated by XRD, TEM, and H_2 chemisorption. Crystallite sizes determined from H_2 chemisorption are smallest, those from TEM intermediate and from XRD highest. This ordering is expected since iron clusters of d < 3 nm of which there could be many, cannot be detected by XRD but can nevertheless adsorb significant quantities of H_2, while TEM averages are based on distributions which weight more heavily the largest crystallites. The order of crystallite size for these three alumina-supported iron catalysts is 10FeA-W > 20FeA-A/E > 10FeA-A/E. These data provide additional evidence that the evaporative deposition method enables preparation of Fe/Al_2O_3 catalysts of higher iron metal dispersion than aqueous-phase impregnation.

Table 4. Comparison of Iron Crystallite Diameters estimated by XRD, TEM, and H_2 Chemisorption

Samples	XRD (nm)	TEM (nm)	H_2 Chemisorption (nm)
10FeA-W	22.8	~20	12.6
10FeA-A/E	9.6	~6	2.6
20FeA-A/E	11.2	~10	3.3

Results and Discussion based on First Principles Calculations
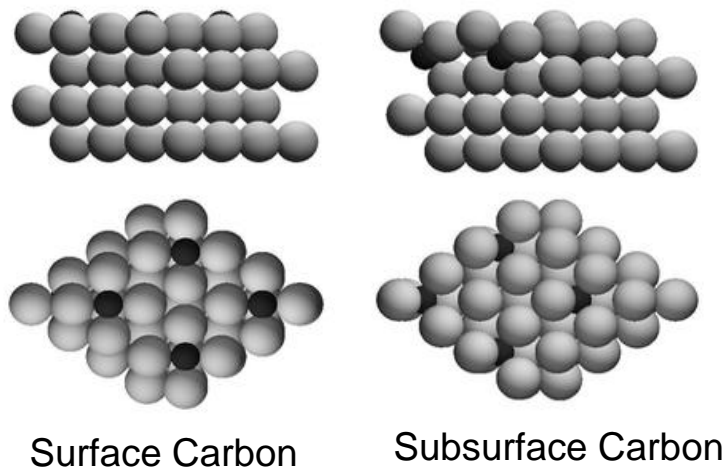
Figure 24 : Binding Energy of surface and subsurface Carbon on Fe(110) at 1/4 ML and 1/8 ML coverages.

Figure 24 provides a cross section and a top view of a Fe(110) slab with the preferred adsorption sites for C both on surface and subsurface. Our calculations suggest that surface C is more stable than subsurface C by about ca. 0.5 eV, both at ¼ ML and 1/8 ML coverages. We note here that most atomic adsorbates lose much more of their stability when they go subsurface, which suggests that creating subsurface C is a relatively facile process, at least in terms of thermochemistry. In the subsequent discussion, we will use the right hand side model shown in Figure 24, whenever we refer to the "subsurface-C Fe(110)" model surface.

Figure 25 shows the results of our detailed calculations for the diffusion of C from the surface of Fe(110) to its first layer in subsurface both in the presence and absence of surface Oxygen (O). While on the clean Fe slab, we find that there is an activation energy barrier more than 1 eV, that barrier drops dramatically in the presence of surface O. This remarkable finding suggests that CO dissociation on Fe(110) producing surface C and O, facilitates the diffusion of C from surface to subsurface enormously, making the formation of Fe-carbides an almost spontaneous process.
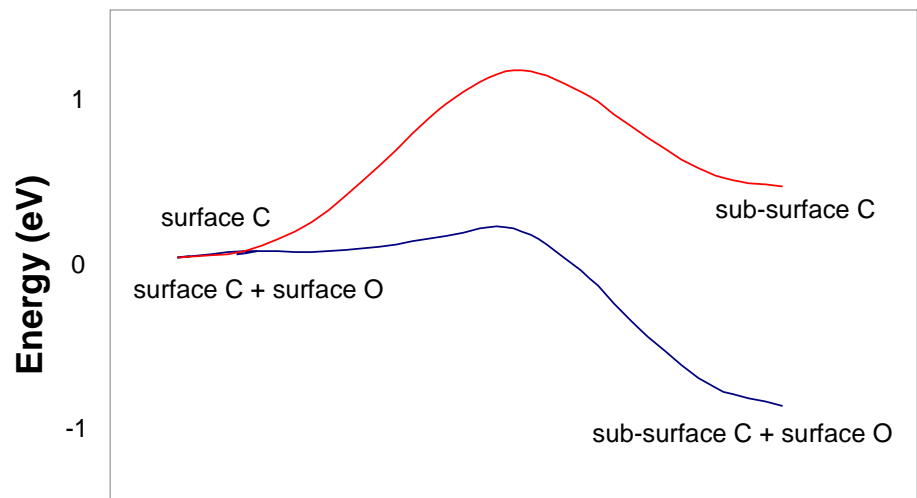

Figure 25 : Reaction coordinate for Diffusion of C from surface to subsurface in the presence and absence of surface O (1/4ML coverage)

Table 5 gives the relative stabilization of various reactive FTS surface intermediates (¼ ML coverage) on a surface with ¼ ML subsurface C when compared to their binding on Fe(110) surface. Subsurface C tends to stabilize all surface-bound intermediates. The magnitude of the stabilization varies between 0.04 and 0.48eV, depending on the surface intermediate.

Table 5 : Relative strength of binding of adsorbates (1/4 ML coverage) on Fe(110) and Fe(110) surface modified by ¼ ML subsurface C, $Fe_C(110)$. All Energies are in eV. Negative values signify stronger binding of adsorbates on $Fe_C(110)$

Species	Energy (eV)
H	-0.15
C	-0.09
O	-0.30
CO	-0.16
CH	-0.24
CH_2	-0.23
CH_3	-0.24
CH_4	-0.04
C_2H_4	-0.48
CCH_3	-0.18
CH_2CH	-0.28

The corresponding stabilization of other surface adsorbates on Fe(110), due to ¼ ML of subsurface C, is provided in Fig. 26 . Among all the surface species studied to date, the largest subsurface-C induced stabilization is for ethylene. That result could have important implications for FTS reaction selectivity on pure Fe versus Fe-carbide catalytic phases.
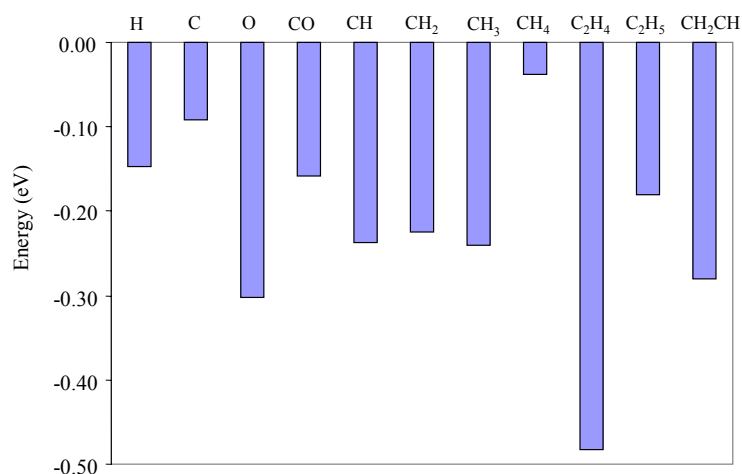
Figure 26 : Subsurface C induced stabilization of surface species (Fe(110) – 1/4 ML coverage)

Figure 27 gives the whole potential energy surface (PES) for the early FTS steps (CO dissociation and C hydrogenation up to CH_4) on the two model surfaces studied: pure Fe(110) and $Fe_C(110)$, the latter having a ¼ ML of subsurface carbon at its preferred site. The main conclusion so far is that subsurface C tends to stabilize all intermediates, and increase the activation energy barriers, as we move to the right of the reaction coordinate. CH_4 formation, in particular, is substantially more activated (i.e.: has a higher barrier) by the presence of subsurface C, which presumably can help in directing reaction selectivity towards higher-C_x products.
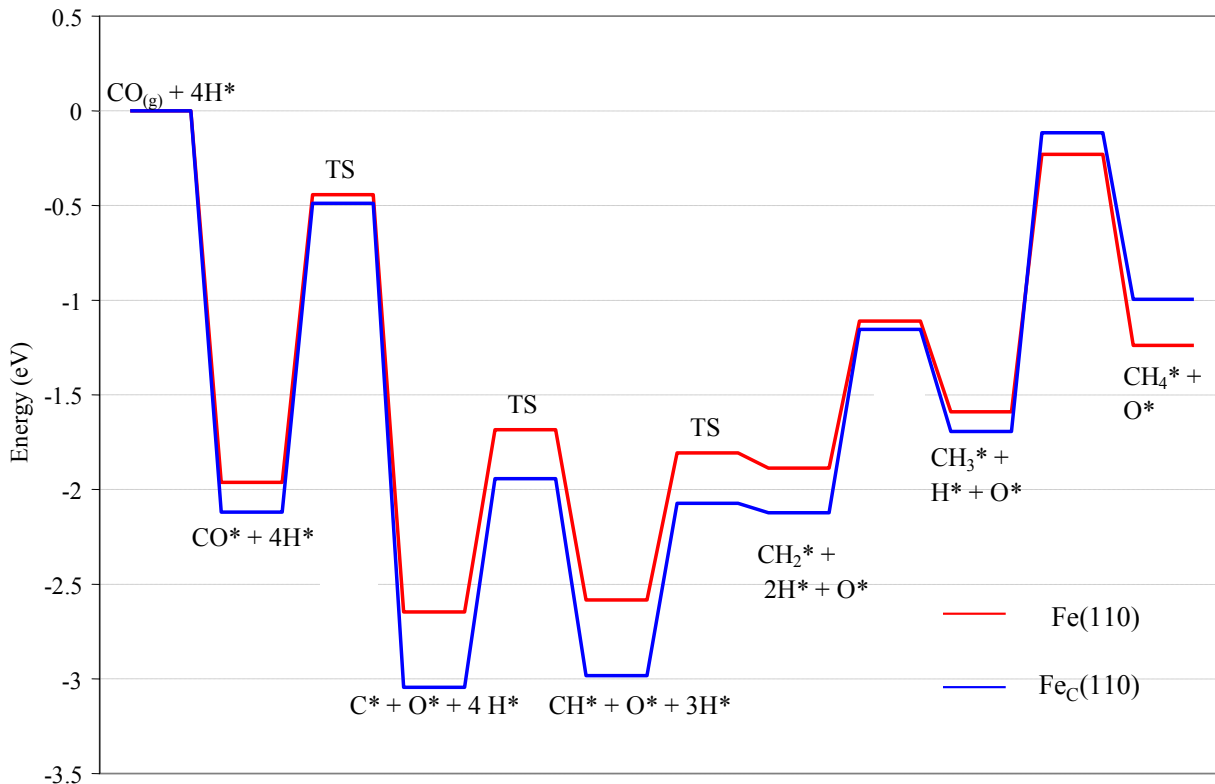
Figure 27 : Potential Energy Surface (thermochemistry and kinetics) for the early FTS steps on Fe(110) and Fe(110) surface modified by 1/4 ML subsurface C, Fe_C(110). Zero of the energy axis corresponds to CO in the gas phases plus four H atoms adsorbed on the corresponding slabs. TS represent Transition States of the respective elementary steps.

Figure 28 extends the comparison made in Figure 27 with the results we got on to two other model surfaces, which we have studied so far. However, in contrast to the data in Fig. 27, data in Fig. 28 provide thermochemistry information only, as we are at the early stages of calculating reaction barriers of the same elementary steps on Co(0001) and particularly on the Pt-modified Fe(110) surface. We anticipate that we will be able to provide a comparison based on a combination of kinetics and thermochemistry on all four surfaces in a later report of our continuing progress. The most important conclusion one can draw from the data shown in Fig. 28 is that Pt destabilizes reactive intermediates compared to both Fe surfaces (i.e.: with or without subsurface C) and brings the whole PES on the Pt-modified surface considerably close to the FTS-PES on Co(0001). It would be interesting to see the effect of Pt on the kinetics of the elementary steps shown here, but also on the remaining steps such as C-C bond formation and hydrogenation of C_2 species. These investigations are within our plans for the second and third year of the present project.
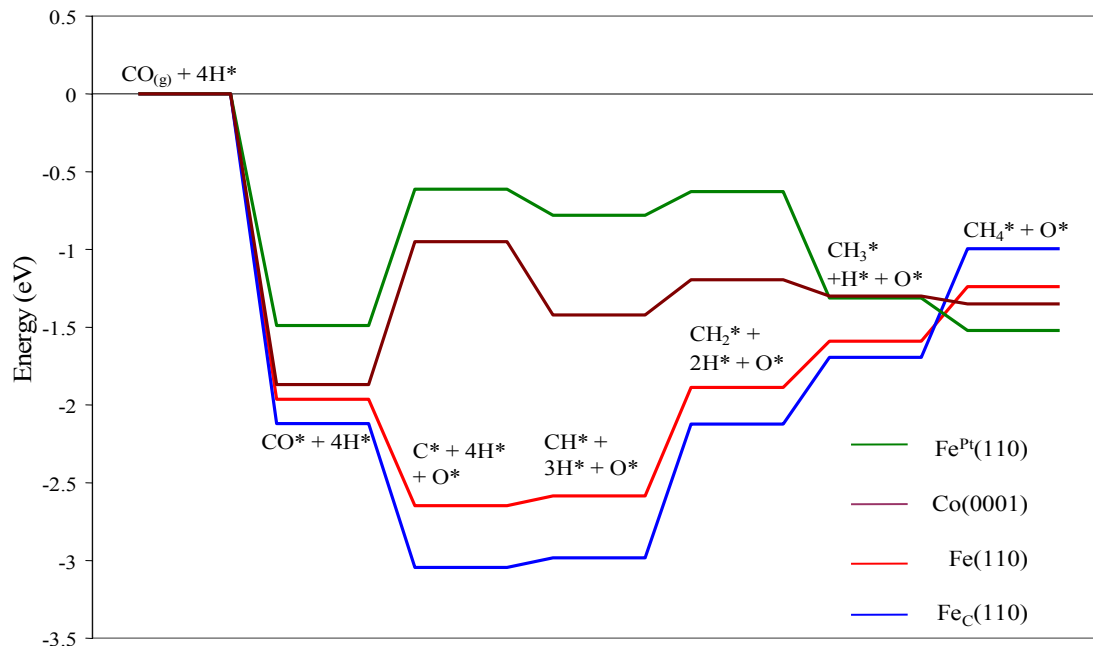
Figure 28 : Potential Energy Surface (thermochemistry only) for the early FTS steps on Fe(110), on Fe(110) surface modified by 1/4 ML subsurface C, or by 1/4 ML surface Pt, and on Co(0001).

During the first year we have also worked on a number of $C - C$ bond forming elementary reaction steps as well as some reactions involving the hydrogenation of C_2 species to yield ethane on the Fe(110) and Fe_C(110) surfaces. Goals for the second and third year include studies of these steps on the Pt-modified Fe surface.

We would like to point out that as we move to steps involving increasingly bigger reactive intermediates and molecules, the calculations become increasingly challenging and demanding in terms of CPU time required. In that regard, any extra computational resources we could access through NETL would be most welcome. When we feel we have developed a solid data set from our computational chemistry studies, we will start putting together a comprehensive microkinetic model in collaboration with BYU, which could bridge the pressure gap for the FTS mechanism on Fe-based catalysts.

Conclusions

A. Conclusions

1. A review of the mechanism and kinetics on FTS reaction on iron catalysts is in progress, from which plausible mechanisms have been developed. The process of preparing this review has enlarged the investigators' knowledge of previous work and their perspective of which mechanistic approaches might prove most fruitful.

2. Three unsupported iron catalysts were successfully prepared by coprecipitation using 1% alumina as a textural promoter; two contained in addition either 1% K or 1% Pt as chemical promoters. The extent of reduction of the 99% Fe/alumina sample is high (90.6%) and its CO/α-Fe adsorption ratio of 0.062 is indicative of a dispersion of 6-10%, which is higher than typically reported for unsupported Fe and is ideal for FTS kinetic studies. These unsupported iron catalysts exhibit very different reduction properties in H_2 and CO atmospheres. Addition of K decreases, whereas addition of Pt increases catalyst's reducibility.

3. 10% Fe/alumina catalysts prepared by evaporative deposition in acetone/ethanol and by aqueous impregnation and then reduced at 300°C were found to have dispersions of 48 and 9.8%. The 48% dispersion is unusually high for a 10% Fe/alumina catalyst. The dispersion of 9.8% is ideal for FTS studies, particular in connection with the UW first-principles studies on Fe(110) based surfaces. However, the unusually high dispersion of the other catalyst is unprecedented and of great interest for design of new FT catalysts. A 20% Fe/alumina was prepared by two-step evaporative deposition in acetone/ethanol solution. The extent of reduction of the catalyst is 45%, which is slightly smaller than two 10%Fe/alumina catalysts. The catalyst reduced at 500ºC has an iron dispersion of 37%. The dispersion is also unusually high for a 20% Fe/alumina catalyst. This catalyst also has unusual thermal stability. The preparation studies provide a basis for preparation of thermally stable catalysts of optimal dispersion and extent of reduction for use in our mechanistic and kinetic studies.

4. Crystallite diameters of supported iron catalysts were estimated by XRD, H_2 chemisorption, and TEM. The order of crystallite size for these three catalysts is 10FeA-W > 20FeA-A/E > 10FeA-A/E. Increasing Fe loading from 10% to 20% using a stepwise impregnation doesn't appear to affect crystallite diameter and extent of reduction significantly. These characterization studies provide a consistent picture of the morphology and dispersion of these catalysts.

5. Our first-principles calculations provided some remarkable insights into the reactivity of Fe(110) surfaces. These calculations strongly suggest that CO dissociation is the rate limiting step for FTS on these surfaces. Subsurface C formation in Fe(110) is almost spontaneous upon CO dissociation on the Fe(110) surface, indicating that the subsurface

C-modified Fe(110) surface might be a more realistic model surface for studying the FTS elementary reaction steps.

6. Subsurface C stabilizes all species adsorbed on the Fe(110) surface. A direct implication of that finding is that gas phase species will preferentially adsorb close to sites with subsurface C in their vicinity, thereby re-enforcing the special role Fe-carbidic phases can play in determining FTS selectivity.

7. According to our DFT calculations, C and CH are the best candidates for the most abundant surface species among all C_1's studied on both the Fe(110) and the subsurface-C-modified Fe(110) surface; CH_2, on the other hand, is rather unstable. In contrast with these findings, our preliminary results on the Pt-modified Fe(110) surface indicate that CH_2 species is more stable and as a result they may be involved in $C - C$ bond formation steps. This could help in explaining the relatively better FTS product distribution observed experimentally over Pt-promoted Fe-based FTS catalysts.

B. Schedule of Tasks

Table 4. Schedule of Tasks

Task	0-6 mo	7-12 mo	13-18 mo	19-24 mo	25-30 mo	31-36 mo
Task 1. Find kinetic parameters and incorporate in model	███	███	███	███	███	███
Task 2. Measure kinetic parameters for key elementary steps						
a. Rebuild TPD system and prepare catalysts	███	███	███	███		
b. TPD, TPSR measurements			███	███		
c. Isotopic study				███	███	
Task 3. DFT studies of elementary steps on selected surface models	███	███	███	███	███	███
Task 4. Collection of rate and selectivity data						
a. Rebuild Berty reactor system	███	███	███			
b. Measure rates and selectivities			███	███		
Task 5. Collaborate, write proposals			███	███	███	███
Reports	▲	▲	▲	▲	▲	▲
Contractor Meeting		■		■		■

References

1. G. P. Van der Laan, A. A. C. M. Beenackers "Kinetics and selectivity of the Fischer-Tropsch synthesis: A literature review" Catal. Rev. –Sci. Eng. 41 (1999) 255-318.

2. C.H. Bartholomew and R. J. Farrauto, *Fundamentals of Industrial Catalytic Processes*, John Wiley, 2005.

3. N. Koga, S. Takemoto, S. Okada, and H. Tanaka, "A kinetic study of the thermal decomposition of iron(III) hydroxide oxides. Part 1. α-FeO(OH) in banded iron formations" Thermochimica Acta 254 (1995) 193-207.

4. A.J.H.M. Kock, H.M. Fortuin, and J.W. Geus, "The Reduction Behavior of Supported Iron Catalysts in Hydrogen or Carbon Monoxide Atmospheres,"

5. G. Neri, A. M. Visco, S. Galvagno, A. Donato, and M. Panzalorto, "Au/iron oxide catalysts: temperature programmed reduction and X-ray diffraction characterization" Thermochimica Acta 329 (1999) 39-46.

6. H. Y. Lin, Y. W. Chen, and C. P. Li, "The mechanism of reduction of iron oxide by hydrogen" Thermochimica Acta 400 (2003) 61-67.

7. A. Basinska, W. K. Jozwiak, J. Goralski, and F. Domka, "The behaviour of Ru/Fe$_2$O$_3$ catalysts and Fe$_2$O$_3$ supports in the TPR and TPO conditions" Appl. Catal. A 190 (2000) 107-115.

8. S. D. Jackson, J. Willis, G. D. McLellan, et. al. "Supported Metal Catalysts: Preparation, Characterization, and Function" J. Catal. 139 (1993) 191-206.